ARMY RESEARCH LABORATORY

# Analytical Prediction of Trajectories for High-Velocity Direct-Fire Munitions

**by Paul Weinacht, Gene R. Cooper, and James F. Newill**

**ARL-TR-3567** **August 2005**

## NOTICES

### Disclaimers

The findings in this report are not to be construed as an official Department of the Army position unless so designated by other authorized documents.

Citation of manufacturer's or trade names does not constitute an official endorsement or approval of the use thereof.

Destroy this report when it is no longer needed. Do not return it to the originator.

**Army Research Laboratory**
Aberdeen Proving Ground, MD 21005-5066

**ARL-TR-3567** **August 2005**

# Analytical Prediction of Trajectories for High-Velocity Direct-Fire Munitions

**Paul Weinacht, Gene R. Cooper, and James F. Newill**
**Weapons and Materials Research Directorate, ARL**

| REPORT DOCUMENTATION PAGE | Form Approved OMB No. 0704-0188 |
|---|---|



| 1. REPORT DATE *(DD-MM-YYYY)* | 2. REPORT TYPE | 3. DATES COVERED (From - To) |
|---|---|---|
| August 2005 | Final | 2003–2005 |

| 4. TITLE AND SUBTITLE | 5a. CONTRACT NUMBER |
|---|---|
| Analytical Prediction of Trajectories for High-Velocity Direct-Fire Munitions | 5b. GRANT NUMBER |
| | 5c. PROGRAM ELEMENT NUMBER |

| 6. AUTHOR(S) | 5d. PROJECT NUMBER |
|---|---|
| Paul Weinacht, Gene R. Cooper, and James F. Newill | 1L1612618AH |
| | 5e. TASK NUMBER |
| | 5f. WORK UNIT NUMBER |

| 7. PERFORMING ORGANIZATION NAME(S) AND ADDRESS(ES) | 8. PERFORMING ORGANIZATION REPORT NUMBER |
|---|---|
| U.S. Army Research Laboratory<br>AMSRD-ARL-WM-BC<br>Aberdeen Proving Ground, MD 21005-5066 | ARL-TR-3567 |

| 9. SPONSORING/MONITORING AGENCY NAME(S) AND ADDRESS(ES) | 10. SPONSOR/MONITOR'S ACRONYM(S) |
|---|---|
| | 11. SPONSOR/MONITOR'S REPORT NUMBER(S) |

**12. DISTRIBUTION/AVAILABILITY STATEMENT**

Approved for public release; distribution is unlimited.

**13. SUPPLEMENTARY NOTES**

**14. ABSTRACT**

An analysis of the velocity-time-range equations for direct-fire munitions has been performed. The analysis characterizes these munitions in terms of three parameters: muzzle velocity, muzzle retardation (or velocity fall-off), and a single parameter defining the shape of the drag curve. Using firing tables drag data for a variety of munitions, the expected range of values of the single parameter defining the shape of the drag curve in the supersonic flight regime has been determined. From the simplified analysis, many important flight characteristics can be determined. These include the velocity-time-range relationships, change in impact velocity due to change in muzzle velocity, gravity drop, change in impact location due to muzzle velocity and muzzle retardation variability, and crosswind deflection. The analysis shows that the muzzle velocity and muzzle retardation are the dominant terms defining these relationships. The shape of the drag curve is shown to be a higher-order effect which, in some cases, can be neglected. To validate these relationships, comparisons are made with numerical trajectory predictions for fielded direct-fire munitions using the measured drag data.

**15. SUBJECT TERMS**

aerodynamics, projectile flight mechanics, pitch-damping

| 16. SECURITY CLASSIFICATION OF: | | | 17. LIMITATION OF ABSTRACT | 18. NUMBER OF PAGES | 19a. NAME OF RESPONSIBLE PERSON |
|---|---|---|---|---|---|
| a. REPORT | b. ABSTRACT | c. THIS PAGE | | | Paul Weinacht |
| UNCLASSIFIED | UNCLASSIFIED | UNCLASSIFIED | UL | 72 | 19b. TELEPHONE NUMBER (*Include area code*)<br>410-278-4280 |

## Contents

## List of Figures

## List of Tables

## Acknowledgments

The authors wish to acknowledge Barbara Tilghman and Fran Mirabelle of the U.S. Army Armament Research, Development, and Engineering Center Firing Tables Branch for assistance in obtaining drag data for a variety of direct-fire munitions. These data were invaluable for establishing the validity of the power law drag relations in the supersonic regime.

# 1. Introduction

The analysis and prediction of the trajectory of projectiles has been a subject investigated for many centuries and is still a topic of interest today. The interest and advancement of the problem has come from two fields: mathematics and physics. As a mathematical problem, the focus has been on the methods for solution of the governing equations. Some of the most noted mathematicians and physicists of the past several centuries, such as Galileo, Bernoulli, and Euler, have investigated the mathematical solution of this problem and have obtained technical advances important for trajectory prediction. To accurately determine the trajectory of a projectile, one must also properly account for the physical effects such as gravity and the air resistance or drag of the projectile. In additional to his laws of motion, Newton has also been credited for the development of the quadratic law of resistance characterizing the aerodynamic drag of a body. Further advances have shown that more sophisticated characterization of the drag is required to predict the trajectory across the complete flight regime of many projectiles.

Over a century ago, Mayevski found that it was possible to express the drag of a projectile as proportional to a power of the velocity within restricted velocity regimes (*1*). This has been described as the Mayevski Law of Resistance (*2*). Piecing together the drag in adjacent velocity regimes using this approach allowed the drag to be characterized over the complete flight regime. Mayevski's advance led to further developments in trajectory prediction methods. One of the more famous methods is the Siacci method. (McCoy [*3*] contains a detailed description of the Siacci method along with additional bibliographic information.) The Siacci method was widely used to predict the flat-fire trajectories for decades after its initial development. The method still has some adherents in the sporting and ammunition community (*3*).

With the advent of the computer, the Siacci method has been replaced by more modern numerical methods. These methods allow rapid and accurate computation of the projectile's trajectory provided the physical characteristics of the projectile (such as the drag) and the atmosphere are appropriately modeled. Modern aerodynamic analysis and trajectory programs such as Prodas (*4*) and AP02 (*5*) provide an excellent means of accurately determining the flight behavior of specific designs.

The increased sophistication of trajectory prediction methods has some unfortunate consequences. The user must often provide an array of details that may or may not be relevant to the answer that is being sought. Additionally, these methods often obscure critical insights into the relationship between important parameters that produce the physical behavior of interest. For example, there are occasions where the aeroballistician would like to be able to predict aspects of the flight trajectory without completely defining the geometry or aerodynamic characteristics of a projectile, such as in preliminary design or experimental testing. In these cases, simplified

analyses can provide accurate results with the minimum amount of relevant input from the user and provide the designer with a clearer understanding of the primary design variables.

For high-velocity direct-fire munitions, it is possible to define aspects of the flight trajectory using simple analytical expressions based on the flat-fire point-mass trajectory equations using a power-law drag relation. Texts on exterior ballistics (*3*, *6*, and *7*) include some of these solutions, although their original source is somewhat unclear. From a mathematical perspective, these closed-form solutions can be obtained using routine analytical methods for solving ordinary differential equations. McCoy (*3*) provides a detailed explanation of the flat-fire assumption and the resulting simplified equations of motion. McCoy (*3*) also provides solutions of the trajectory equations for three special cases including the variation of the drag coefficient with the inverse of the Mach number, the variation of the drag coefficient with the inverse of the square root of the Mach number, and for constant drag coefficient. The later two solutions were previously published by McShane et al. (*6*).

Solutions of the flat-fire equations of motion using a power-law drag relation with a variable parameter for the power-law exponent have also been obtained (*7*–*9*). These solutions were an important component of early implementations of the Siacci method (*8*, *9*). The previously mentioned solution (*3*, *6*) where the drag varies with the inverse of the square root of the Mach number is also a special case of the more general solution which allow a variable power-law exponent.

Using these solutions, it can be shown that the projectile trajectory and velocity history can be characterized in terms of three parameters: the projectile's muzzle velocity, a parameter related to the muzzle retardation, and a single parameter defining the shape of the drag curve. Characterizing the trajectory in terms of these parameters has been shown previously by other investigators (*7*, *10*), although the particular definition of the parameters related to the muzzle retardation differ somewhat from the definition used here. It is believed that the definition used here may be more appropriate for modern high-velocity munitions. Using these three parameters, a wide range of trajectory characteristics can be determined, including the velocity-time-range relationships, the wind sensitivity of the projectile, gravity drop, gun elevation angle to hit a target at range, and the sensitivity of the vertical impact location to changes in muzzle velocity and projectile drag coefficient or retardation. The results presented here also show that trajectory parameters can be scaled using the muzzle velocity and muzzle retardation allowing the various trajectory characteristics to be presented as a universal family of curves valid for a wide range of munition types and sizes.

These relations can be developed using the point-mass equations of motion. These equations of motion are obtained from Newton's second law. The flat-fire point-mass equations also assume that the transverse aerodynamic forces such as the lift and Magnus forces are small and that the Coriolis acceleration due to the earth's rotation can be neglected. Neglecting the transverse

aerodynamic forces is typically a good assumption if the total yaw of the projectile is small. The point-mass equations of motion for a projectile are written as follows:

$$m\frac{dV_x}{dt} = -\frac{1}{2}\rho V^2 S_{ref} C_D \frac{V_x}{V}. \tag{1}$$

$$m\frac{dV_y}{dt} = -\frac{1}{2}\rho V^2 S_{ref} C_D \frac{V_y}{V} - mg. \tag{2}$$

$$\frac{ds_x}{dt} = V_x. \tag{3}$$

$$\frac{ds_y}{dt} = V_y. \tag{4}$$

The initial conditions are

$$V_x(t = t_0) = V_0 \cos\theta_0, \tag{5}$$

$$V_y(t = t_0) = V_0 \sin\theta_0, \tag{6}$$

$$s_x(t = t_0) = s_{x0}, \tag{7}$$

and

$$s_y(t = t_0) = s_{y0}. \tag{8}$$

The current report presents analytical solutions based on approximations valid for high velocity direct-fire or flat-fire munitions. The flat-fire assumption allows the point-mass equations, which are, in the general case, nonlinear and coupled, to be decoupled and solved independently. By considering high velocity supersonic flight, the drag coefficient can be modeled as a simple function of the Mach number. The particular functional form of the drag coefficient allows variations in the shape of the drag curve to be considered parametrically.

In this report, discussion of the functional form for the drag coefficient is first presented along with parametric values defining the drag curves for current munitions. The point-mass equations are then combined to yield equations in terms of the total velocity of the projectile. These equations are described here as the 1-DOF (degree of freedom) point-mass equations. Using the functional form for the drag coefficient, analytical solutions for the 1-DOF point-mass equations are presented. Using these results, the solutions of the 2-DOF point-mass equations (equations 1–8) are then presented. The approach is then validated by comparing the results obtained from the analytic method with numerical trajectory predictions made using actual drag data.

## 2. Functional Form for the Drag Coefficient

The solution of the equations of motion requires the projectile drag to be defined. For a fixed geometry, the drag coefficient is a function of the nondimensional flight velocity or Mach number. (The drag coefficient may also be considered to exhibit some dependence on the Reynolds number; however, it is assumed here that the Reynolds number based on the freestream speed of sound is constant and the effects of Reynolds number are implicitly included in the drag coefficient variation with Mach number. The drag coefficient can also depend on the wall temperature. Nominal wall temperature effects are considered to be implicitly included in the drag coefficient and variations from the nominal conditions are not considered here.) A typical drag curve is shown schematically in figure 1. There are three critical regions on the drag curve. In the subsonic region ($M < 0.8$), the drag coefficient is relatively constant. In the transonic regime ($0.8 < M < 1.2$), the drag coefficient is characterized by a sharp rise with increasing Mach number. In the supersonic region, the drag coefficient decreases in an asymptotic manner as the Mach number increases. To accurately predict the projectile velocity as a function of range or time across the entire flight regime, the entire drag curve must be utilized. However, in many cases, only the supersonic flight regime may be of interest, and a simplified form of the drag curve may be utilized.

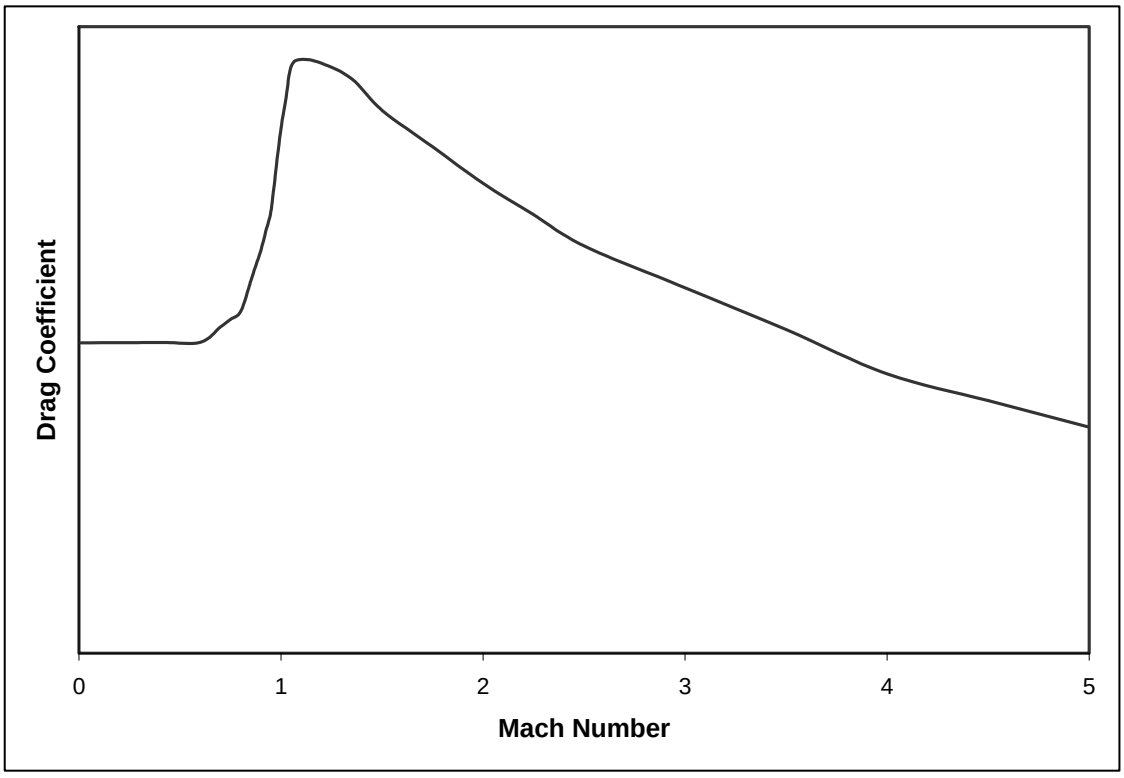


Figure 1. Schematic of a typical drag curve.

As previously discussed, Mayevski found that it was possible to express the drag of a projectile as proportional to a power of the velocity within restricted velocity regimes (*1*). Such an approach has been adopted here. Other researchers have noted similar behavior of the drag coefficient in the supersonic regime. Thomas (*11*) reported that several researchers noted that the behavior of the drag coefficient of some projectiles in the supersonic regime varies with the inverse of the square root of the Mach number. This has been described as the "3/2" law of resistance as the dimensional drag varies with the 3/2 power using this form of the drag coefficient. Thomas also proposed his own form of the drag coefficient in the supersonic regime. However, the approach has gained little acceptance and its implementation in the context of the analysis presented here adds additional complexity that is not warranted.

More recently, Celmins (*12*) noted that the velocity decay or retardation of many high-velocity munitions was relatively constant and conjectured that the supersonic drag coefficient of many projectiles appears to vary with the inverse of the Mach number above Mach 2.5. Further investigation performed as part of the current study suggests that a more general power-law drag law can be utilized which improves the accuracy of the trajectory simulations and highlights the relative insensitivity of the results to this generalized form.

In the current investigation, the drag coefficient is assumed to vary with the inverse of the velocity (or Mach number) raised to a power "n" as shown in equation 9.

$$C_D \propto \frac{1}{M^n} \propto \frac{1}{V^n}. \tag{9}$$

The Mach number and velocity are proportional to each other for a constant freestream speed of sound. In the context of the current analysis, a constant freestream speed of sound is expected due to the fixed atmospheric conditions encountered in flat fire. Using this functional form, the drag coefficient can be expressed in terms of the launch drag coefficient $C_D\big|_{V_0}$ and the ratio of the instantaneous velocity $V$ to the muzzle velocity $V_0$.

$$C_D = C_D\big|_{V_0}\left(\frac{V_0}{V}\right)^n. \tag{10}$$

Modeling the drag in this fashion does not allow the yaw drag effect to be considered unless it is implicitly part of the drag curve. To define the possible range of exponents, U.S. Army firing tables "aeropack" data for a variety of gun-launched munitions was utilized. This data contains the drag coefficient data used to develop firing tables for U.S. Army munitions and represents a definitive source of drag data based on the most current data available. Table 1 presents the drag coefficient exponent determined for various munitions. This exponent represents the best fits of the drag data over the range between the muzzle velocity and Mach 2.5. Curve fits were also performed over the entire supersonic regime, and some slight differences (typically a slight decrease) in the drag coefficient exponent were noted. However, it was determined that for

many of the munitions currently of interest, the projectile velocity did not decrease below Mach 2.5 over the effective range of the projectile and only the representative exponent for this range of velocities is shown here.

Table 1. Drag coefficient exponents for various munitions.

| Munition | Caliber (mm) | Geometry | Exponent |
|---|---|---|---|
| M829 | 120 | Cone-cylinder-fins | 0.89 |
| M829A1 | 120 | Cone-cylinder-fins | 0.80 |
| M830A1 | 120 | Cone-cylinder-tailboom | 0.74 |
| M865PIP | 120 | Cone-cylinder-flare | 0.92 |
| M865E3 | 120 | Cone-cylinder-flare | 0.78 |
| XM1002 | 120 | Cone-cylinder-flare | 0.82 |
| M791 | 25 | Cone-cylinder-boattail | 0.99 |
| M193 | 5.56 | Ogive-cylinder-boattail | 0.40 |
| M392A2 | 105 | Ogive-cylinder-boattail | 0.58 |

A variety of munitions were selected in the results presented in table 1 based on differences in their shapes and sizes. The exponents varied between 0.40 and 0.99, with the mean about 0.77. Clearly, the drag coefficient exponent is dependent on the munition type and the drag does not vary with the inverse of the Mach number as suggested by Celmins (*12*).

The results of analyzing the drag curves for each of these munitions indicate that the drag can accurately be represented by the form shown in equation 10. For example, the drag curve for the M829 kinetic energy projectile is shown in figure 2. Over the range between the muzzle velocity (M = 4.85) and M = 2.5, the drag curve is well represented by the form shown in equation 10 with the exponent of n = 0.89. If the curve is further extrapolated below M = 2.5, some additional error is noted. These errors can be addressed with alternative fits to the data curve. However, this fit should be sufficient over the effective range of this munition.

Another source of drag data which is available to examine the variation of the drag coefficient with Mach number is the standard axisymmetric projectile shapes that were tested in the early to mid-1900's. The resulting drag curves are referred to as the Ingalls, G1, G2, G5, G6, G7, and G8 drag curves. McCoy (*3*) contains a compilation of each of these drag function along with a tabulation of the drag curve for spherical projectiles. Using this set of data, the exponent defining the shape of the drag variation with Mach number was determined from a least-squares fit of the drag data over the range between Mach 1.5 and 3.0 in a manner similar to that previously described. The resulting exponents are shown in table 2.

The Ingalls and G1 drag functions represent the drag curve for the same projectile geometry, but represent two interpretations of the drag data. Both drag functions are similar over the Mach 1.5 to 3.0 interval and have the same exponent representing the shape of the drag curve. Above Mach 3, both drag coefficient variations diverge somewhat with the G1 drag function showing much less of a variation with Mach number. The Ingalls drag function shows a variation above

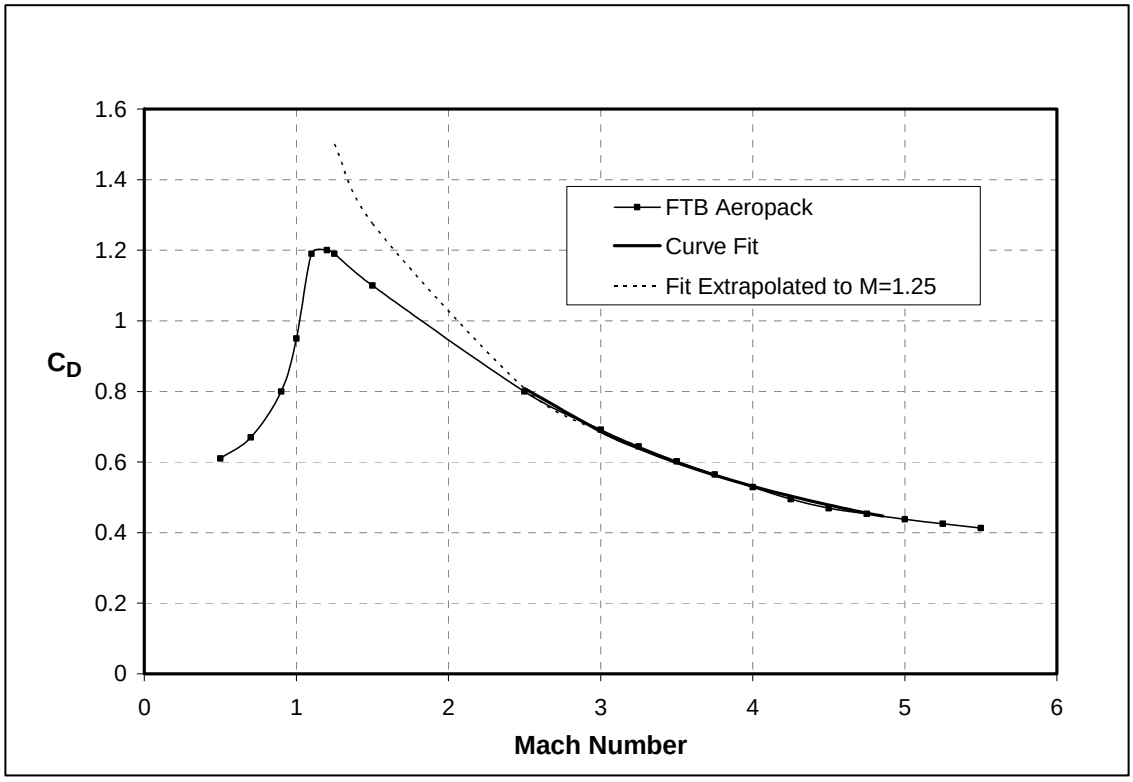


Figure 2. Fit of drag coefficient for the M829.

Table 2. Drag coefficient exponents for various drag functions.

| Drag Function | Geometry | Exponent |
|---|---|---|
| Ingalls | Short ogive-cylinder | 0.36 |
| G1 | Short ogive-cylinder | 0.36 |
| G2 | 10° cone-cylinder-boattail | 0.62 |
| G5 | Ogive-cylinder-boattail | 0.59 |
| G6 | Ogive-cylinder | 0.85 |
| G7 | Ogive-cylinder-boattail | 0.51 |
| G8 | Ogive-cylinder | 0.71 |
| Spherical | Spherical Ball | 0.08 |

Mach 3 that is more consistent with the variation between Mach 1.5 and 3.0 and is better represented by the exponent obtained from the fits than the G1 drag function. It should be noted that the G1 drag function is currently utilized by many sporting industry ammunition manufacturers as the standard representation of the shape of the drag curve for their projectiles, although the actual magnitude of the drag coefficient is adjusted through a form factor in the ballistic coefficient quoted for each projectile type (see McCoy [*3*] for details).

The G2, G5, G6, G7, and G8 drag functions display slightly different variations in the drag coefficient exponent in the Mach 1.5 to 3.0 regime and are generally similar in magnitude to the

exponents shown previously in table 1. The spherical projectile shows relatively little variation drag coefficient in the supersonic regime as represented by the low value of the drag coefficient exponent.

## 3. Solution of the 1-DOF Equations

The point-mass equations shown previously in equations 1–8 are useful for predicting the ballistic trajectory of a projectile. However, there are instances where the total velocity rather than the two-dimensional velocity components is desired. In this case, the point-mass equations can be recast in terms of the total projectile velocity V.

$$V = \sqrt{V_x^2 + V_y^2} \ . \tag{11}$$

$$m\frac{dV}{dt} = -\frac{1}{2}\rho V^2 S_{ref} C_D - mg\frac{V_y}{V} . \tag{12}$$

The presence of the vertical velocity component $V_y$ in equation 12 requires an additional equation (equation 2, for instance) to obtain a complete set of equations. For flat fire, the gravity term in equation 12 is much smaller than the drag term and can be ignored as shown:

$$m\frac{dV}{dt} = -\frac{1}{2}\rho V^2 S_{ref} C_D . \tag{13}$$

The result is a single equation which can be solved for the total velocity provided that the functional form for the drag coefficient is known. In many practical situations, if the gun elevation is less than 10°, equation 13 provides accurate evaluations of the total velocity. This implies that the velocity history itself is independent of gun elevation under these same conditions.

The arc length along the flight path, s, is related to the total velocity of the projectile V by the following differential equation:

$$\frac{ds}{dt} = V . \tag{14}$$

However, the arc length is not normally a quantity used in describing the projectile trajectory. A more convenient coordinate is the horizontal range coordinate $s_x$. For flat-fire trajectories, the horizontal range coordinate is nearly equal to the arc length and the approximations shown in equations 15 and 16 can be made with little loss of accuracy.

$$s \cong s_x . \tag{15}$$

$$\frac{ds_x}{dt} \cong V \,. \tag{16}$$

Equations 13 and 16 are referred to as the 1-DOF equations.

Using equation 16 and applying the chain rule, an alternative form of equation 13 can be obtained that is useful in determining the total velocity as a function of range.

$$mV\frac{dV}{ds_x} = -\frac{1}{2}\rho V^2 S_{ref} C_D \,. \tag{17}$$

The functional form of the drag coefficient presented previously in equation 10 can be substituted into equations 13 and 17 to obtain the following equations of motion:

$$\frac{d(V/V_0)}{dt} = \left(\frac{dV}{ds}\right)_0 \left(\frac{V_0}{V}\right)^{n-2} . \tag{18}$$

$$\frac{d(V/V_0)}{ds_x} = \frac{1}{V_0}\left(\frac{dV}{ds}\right)_0 \left(\frac{V_0}{V}\right)^{n-1} . \tag{19}$$

Here, $\left(\frac{dV}{ds}\right)_0$ is the retardation (or velocity fall-off) of the projectile evaluated at the muzzle.
The muzzle retardation is related to the drag coefficient as shown in equation 20.

$$\left(\frac{dV}{ds}\right)_0 = -\frac{1}{2m}\rho V_0 S_{ref} C_D\big|_{V_0} \,. \tag{20}$$

It is important to note that the form of equations 18 and 19 shows that the velocity history of the projectile can be characterized in terms of three parameters: the muzzle velocity, the muzzle retardation, and the exponent characterizing the shape of the drag curve.

### 3.1 Velocity-Time-Range Relations

Equations 18 and 19 can be integrated to obtain closed form solutions of the governing equations. These are shown as follows:

$$\frac{V}{V_0} = \left\{1 + n\left(\frac{dV}{ds}\right)_0 \frac{(s_x - s_{x0})}{V_0}\right\}^{\frac{1}{n}} \quad n \neq 0 \,. \tag{21}$$

$$\frac{V}{V_0} = \exp\left\{\left(\frac{dV}{ds}\right)_0 \frac{(s_x - s_{x0})}{V_0}\right\} \quad n = 0 \,. \tag{22}$$

$$\frac{V}{V_0} = \left\{1 + (n-1)\left(\frac{dV}{ds}\right)_0 (t - t_0)\right\}^{\frac{1}{n-1}} \quad n \neq 1. \tag{23}$$

$$\frac{V}{V_0} = \exp\left\{\left(\frac{dV}{ds}\right)_0 (t - t_0)\right\} \quad n = 1. \tag{24}$$

The validity of these solutions is limited to regimes where the power-law drag variation is applicable. Generally, for munitions launched at supersonic velocities, these equations are only applicable at velocities above the sonic velocity because of the distinct change in the drag variation near Mach 1, as seen previously in figure 1. Further restrictions on the velocity regime where these equations are valid may be imposed by the applicability of a particular power-law drag variation, as demonstrated previously in figure 2. By considering the physical considerations and practical limitations of these equations, the mathematical limitations that require the bracketed quantities in equations 21 and 23 to be positive to obtain real number solutions can be ignored because they are less restrictive than the physical considerations. It should also be recognized that the constant drag coefficient results (n = 0) are representative of the drag variation in the subsonic regime and these equations can be applied here without the mathematical difficulties previously discussed.

The results in equations 21 and 23 represent the general solutions from which equations 22 and 24, respectively, can be obtained as mathematical limiting cases. These special cases are presented explicitly here (and throughout the report) for completeness, although accurate results can also be obtained for the n = 0 or n = 1 cases using the general solutions with n = 0.01 or n = 0.99, respectively.

Equations relating range to time can be easily obtained by combining equations 21–24.

$$(t - t_0) = \frac{1}{(n-1)\left(\frac{dV}{ds}\right)_0}\left[\left\{1 + n\left(\frac{dV}{ds}\right)_0 \frac{(s_x - s_{x0})}{V_0}\right\}^{1-\frac{1}{n}} - 1\right] \quad n \neq 0, n \neq 1. \tag{25}$$

$$(t - t_0) = \frac{1}{\left(\frac{dV}{ds}\right)_0} \ln\left\{1 + \left(\frac{dV}{ds}\right)_0 \frac{(s_x - s_{x0})}{V_0}\right\} \quad n = 1. \tag{26}$$

$$(t - t_0) = \frac{1}{\left(\frac{dV}{ds}\right)_0}\left[1 - \exp\left\{-\left(\frac{dV}{ds}\right)_0 \frac{(s_x - s_{x0})}{V_0}\right\}\right] \quad n = 0. \tag{27}$$

Similarly, equations for the range as a function time can be derived and are shown in equations 28–30.

$$(s_x - s_{x0}) = \frac{V_0}{-\left(\frac{dV}{ds}\right)_0}\left[1 - \exp\left\{\left(\frac{dV}{ds}\right)_0 (t - t_0)\right\}\right] \quad n = 1. \tag{28}$$

$$(s_x - s_{x0}) = \frac{V_0}{-\left(\frac{dV}{ds}\right)_0} \ln\left\{1 - (t - t_0)\left(\frac{dV}{ds}\right)_0\right\} \quad n = 0. \tag{29}$$

$$(s_x - s_{x0}) = \frac{V_0}{-\left(\frac{dV}{ds}\right)_0 n}\left[1 - \left\{1 + (n-1)\left(\frac{dV}{ds}\right)_0 (t - t_0)\right\}^{\frac{n}{n-1}}\right] \quad n \neq 1, n \neq 0. \tag{30}$$

The results presented in equations 21–30 again show that the velocity, range, and time-of-flight are functions of just three parameters: the muzzle velocity, the muzzle retardation, and the exponent defining the shape of the drag curve. The results also show that the velocity can be nondimensionalized by the muzzle velocity, the range can be nondimensionalized by the ratio of the muzzle velocity to the muzzle retardation, and the time-of-flight can be nondimensionalized by the muzzle retardation. This scaling of the results in terms of these nondimensional parameters produces a family of curves in terms of a single parameter, the exponent defining the shape of the drag curve.

Although equations 21 and 22 are compact, a useful expression can be developed using a Taylor's series expansion. The expansion is valid for all values of the drag coefficient exponent and represents the exact solutions presented in equations 21 and 22 as a single equation.

$$\frac{V}{V_0} = 1 + \left(\frac{dV}{ds}\right)_0 \frac{(s_x - s_{x0})}{V_0} + \frac{1}{2}(1-n)\left\{\left(\frac{dV}{ds}\right)_0 \frac{(s_x - s_{x0})}{V_0}\right\}^2 + .. + \frac{1}{j!}(1-n)(1-2n)...(1-(j-1)n)\left\{\left(\frac{dV}{ds}\right)\frac{(s_x - s_{x0})}{V_0}\right\}^j + ... \tag{31}$$

As can be seen from equation 31, the fractional remaining velocity is to first order in range a function of the retardation at the muzzle and does not depend on the shape of the drag curve. The shape of the drag curve only affects the second order and higher terms of the expansion. It is also noted that the first j + 1 terms of the expansion represent the exact solution for $1/M^{1/j}$ variations in the drag coefficient. The first three terms of the expansion provide excellent accuracy when the exponent for the drag coefficient variation is $0.5 \le n \le 1.25$ and the velocity is between $1 \ge V/V_0 \ge 0.5$. This range of exponents appears to represent typical values for supersonic projectile applications. For applications where the velocity or drag coefficient exponent is outside this range, accurate solutions can be obtained with additional higher order terms if necessary.

Figures 3 and 4 show the fractional remaining velocity as a function of the scaled range for various values of the drag coefficient exponent. For reference, the scaled and dimensional ranges for various notional munition types is shown in table 3. For example, the scaled range of 0.5 corresponds to a range of 13.3 km for a muzzle velocity of 1600 m/s and a retardation of 60 (m/s)/km, which are representative values for modern kinetic energy projectiles. Figures 3 and 4 show the relative effect of the drag coefficient exponent on the velocity decay for a range of exponents from $1/M$ (n = 1) to constant drag coefficient (n = 0). The $1/M$ drag coefficient variation shows a linear variation of the velocity decay with range. For values of the exponent less than 1, the rate of velocity decay decreases with distance downrange.

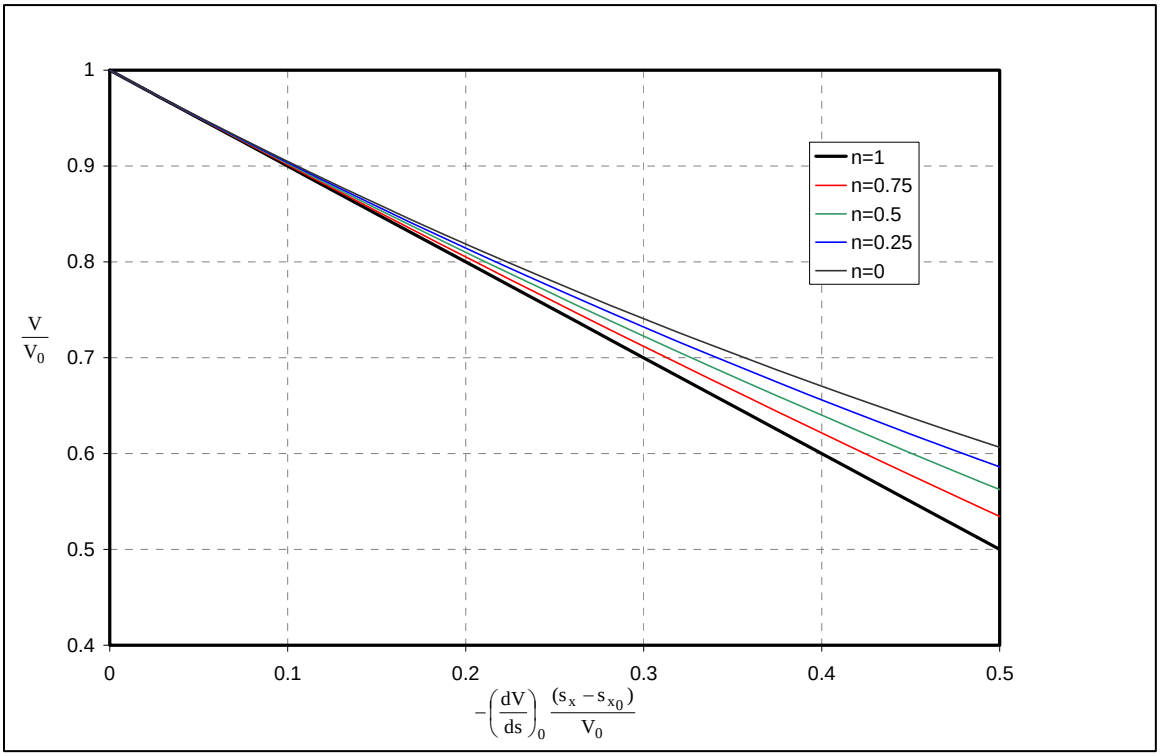


Figure 3. Fractional remaining velocity as a function of scaled range.

For the representative muzzle velocity of 1600 m/s and a retardation of 60 (m/s)/km, the results shown that at 3 km the fractional remaining velocity is 0.888 and 0.894 when the drag coefficient varies with $1/M$ (n = 1) or when the drag coefficient is constant (n = 0), respectively. At 5 km, the fractional remaining velocities decrease to 0.815 and 0.829, for n = 1 and n = 0, respectively. For rounds with these characteristics, it does not appear that shape of the drag curve as defined by the drag coefficient exponent is particularly critical in modeling the velocity decay of the projectile, as reasonable accuracy can be obtained by assuming a constant retardation over ranges of up to 5 km.

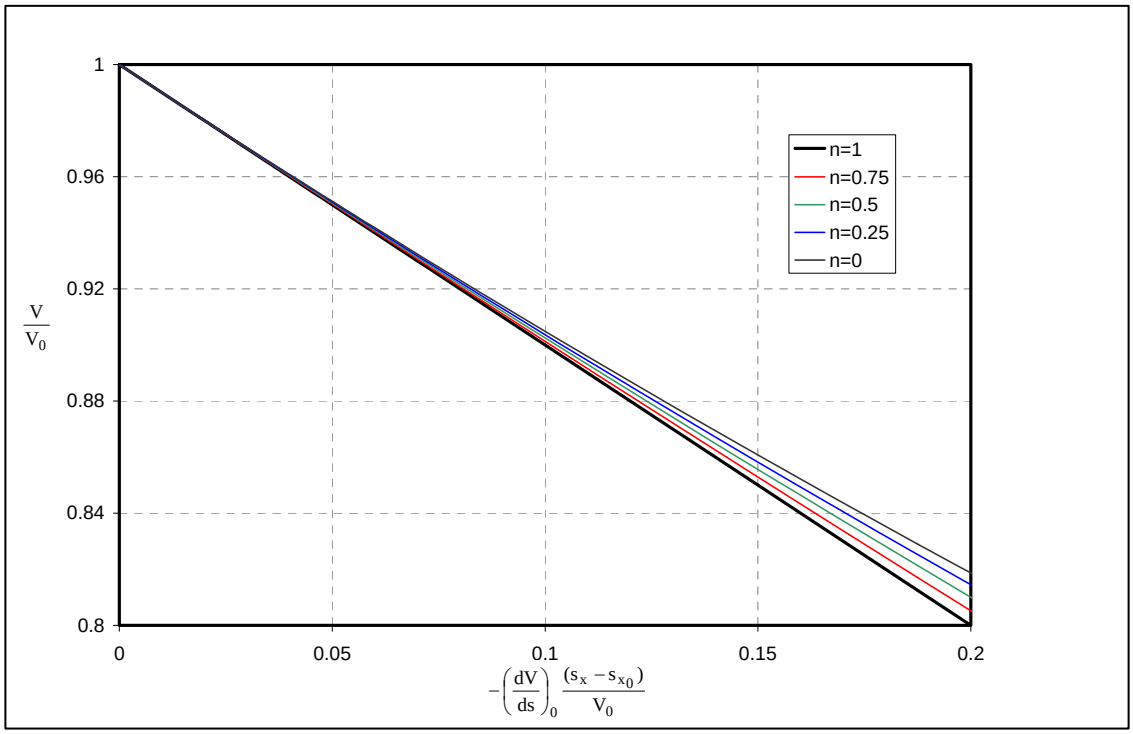


Figure 4. Fractional remaining velocity as a function of scaled range (close-up).

Table 3. Nondimensional ranges for various notional round types.

| **Notional Round Type** | **Muzzle Velocity (m/s)** | **Muzzle Retardation ([m/s]/km)** | **Dimensional Range (km)** | **Nondimensional Range** $-\left(\frac{dV}{ds}\right)_0 \frac{(s_x - s_{x0})}{V_0}$ |
|---|---|---|---|---|
| KE | 1600 | 60 | 3 | 0.1125 |
| | | | 5 | 0.1875 |
| | | | 13 | 0.4875 |
| HEAT | 1100 | 220 | 1 | 0.2 |
| | | | 2.5 | 0.5 |
| KE trainer | 1700 | 340 | 1 | 0.2 |
| | | | 2.5 | 0.5 |
| Small arms | 1000 | 1000 | 0.2 | 0.2 |
| | | | 0.5 | 0.5 |

For training ammunition or high-explosive antitank (HEAT) rounds that have higher retardation, the velocity decay occurs over shorter ranges and the effect of the drag coefficient variation is more apparent. For a notional training munition with a muzzle velocity of 1700 m/s and a retardation of 340 (m/s)/km or a notional HEAT round with a muzzle velocity of 1100 m/s and a retardation of 220 (m/s)/km, the fractional remaining velocity is 0.8 and 0.819 at 1 km and 0.5 and 0.607 at 2.5 km when drag coefficient varies with $1/M$ (n = 1) or when the drag coefficient is constant (n = 0), respectively. It should be noted that a constant drag coefficient (n = 0)

represents an extreme case and the differences in most practical situations will likely be even less if a better estimate of the drag coefficient exponent is available.

The results shown in equation 31 and figures 3 and 4 also explain some of the conjectures regarding the drag behavior of high-velocity projectiles made by Celmins (*12*). These conjectures were based on the velocity vs. range data. The velocity vs. range data examined by Celmins showed a nearly constant rate of decrease in velocity with increasing range which is consistent with a drag coefficient that varies with the inverse of the Mach number. However, the results shown here demonstrate that velocity variation with range is relatively insensitive to the shape of the drag curve. In fact, for many projectiles, it may be very difficult to distinguish the effect of the drag coefficient exponent on the velocity history over the effective range of the projectile.

The Taylor's series expansion of the velocity shown in equation 31 also provides a convenient form for use in analyzing data obtained from range testing. If the variation of the projectile velocity with range is available (from radar data, for instance), equation 31 provides a convenient form for polynomial curve fitting so that the velocity history can be extrapolated to longer ranges. Using a second-order polynomial fit of the form,

$$\frac{V}{V_0} = 1 + a_1(s_x - s_{x0}) + a_2(s_x - s_{x0})^2, \tag{32}$$

allows the muzzle retardation and shape of the drag curve to be determined from the coefficient $a_1$ and $a_2$.

$$\left(\frac{dV}{ds}\right)_0 = \frac{V_0}{a_1}. \tag{33}$$

$$n = 1 - 2\frac{a_2}{a_1^2}. \tag{34}$$

Some caution should be applied if polynomials higher than second order are utilized because there are only three independent parameters describing the velocity history and the higher-order coefficients are not independent. If higher-order polynomials are used, the coefficients of the higher-order terms should be cast in terms of the three parameters as shown in equation 31 so that the curve fitting is consistent with the form shown in equation 31. The curve fitting, as well as any extrapolation of the results to longer ranges, must also be performed in the supersonic regime where the variation of the drag coefficient can be represented by the functional form shown in equation 10.

The variation of retardation with range can be determined from the variation of velocity with range as shown in equation 35.

$$\frac{\left(\frac{dV}{ds}\right)}{\left(\frac{dV}{ds}\right)_0} = \frac{-\frac{1}{2m}\rho V S_{ref} C_D}{-\frac{1}{2m}\rho V_0 S_{ref} C_D\big|_{V_0}} = \left(\frac{V}{V_0}\right)^{1-n} . \tag{35}$$

An alternative form of the variation of the retardation with range can be obtained from equation 35 by taking the derivative of the velocity with respect to range to obtain the following expression.

$$\frac{\frac{dV}{ds}}{\left(\frac{dV}{ds}\right)_0} = 1 + (1-n)\left(\frac{dV}{ds}\right)_0 \frac{(s_x - s_{x0})}{V_0} + \frac{1}{2}(1-n)(1-2n)\left\{\left(\frac{dV}{ds}\right)_0 \frac{(s_x - s_{x0})}{V_0}\right\}^2 + \ldots$$

$$+ \frac{1}{j!}(1-n)(1-2n)\ldots(1-j\cdot n)\left\{\left(\frac{dV}{ds}\right)_0 \frac{(s_x - s_{x0})}{V_0}\right\}^j + \ldots \tag{36}$$

As shown in equation 36, the retardation is constant throughout the trajectory for a drag coefficient exponent of one. The drag coefficient exponent appears in the first order and higher terms of the expansion. Thus, the relative importance of the shape of the drag curve should be more apparent in the retardation than in the velocity history. Of course, this would be expected since the drag coefficient is directly related to the retardation as shown in equation 20.

Figure 5 shows the variation of retardation with range for various values of the drag coefficients exponent. As previously noted, the retardation is constant with range for a drag coefficient exponent of one. For drag coefficient exponents less than one, the retardation decreases with increasing range.

The definition of retardation used in equations 20 and 35 is widely accepted at this point in time, although alternative definitions of retardation exist in the literature. More traditional texts (*8*, *13*) often define the retardation as shown in equation 37.

$$R = \left(\frac{dV}{dt}\right) = \frac{1}{2m}\rho S_{ref} C_D V^2 = \left(\frac{dV}{dt}\right)_0 \left(\frac{V}{V_0}\right)^{n-2} . \tag{37}$$

This is essentially the ratio of the drag force to the mass and represents the change in velocity per unit time of flight. Generally speaking, this form of the retardation is a function of the flight velocity across the flight regime. Because of its strong dependence on velocity, this parameter is less useful in characterizing the flight characteristics of a munition than the definition in equation 20.

Other references (*7*, *9*) utilize a retardation coefficient that has a form (or its reciprocal) shown in equation 38.

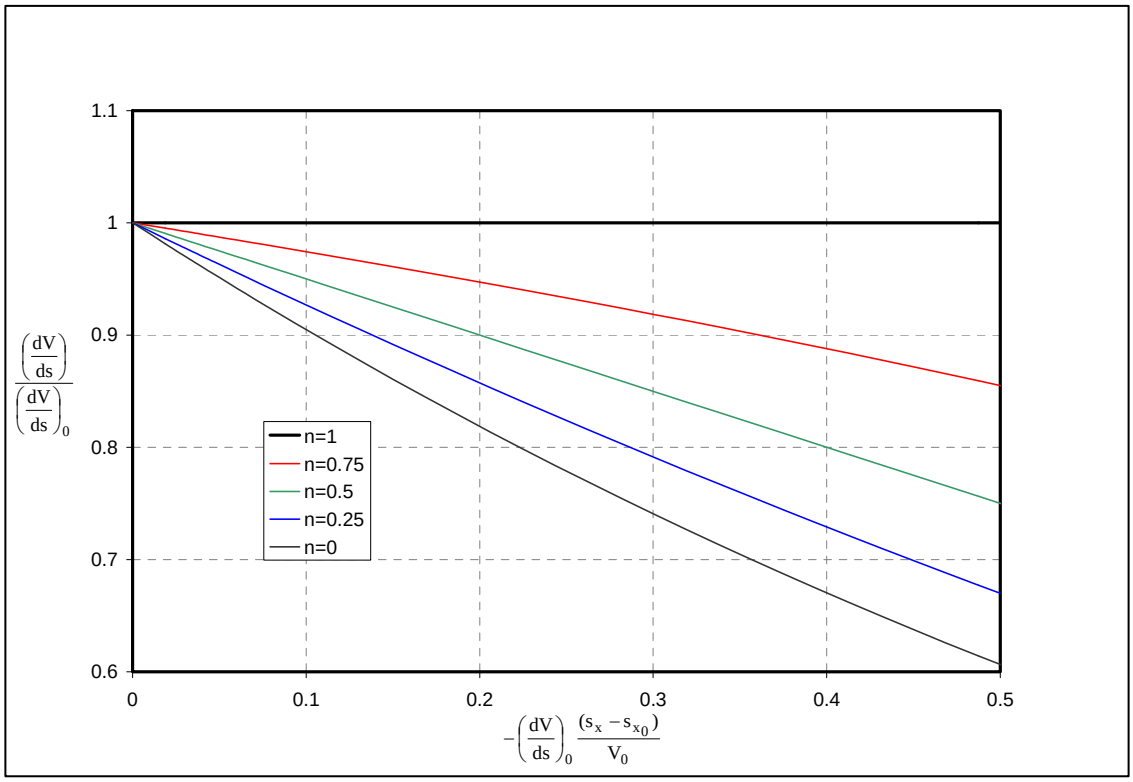


Figure 5. Retardation as a function of scaled range.

$$\hat{R} = \frac{1}{V}\left(\frac{dV}{ds}\right) = \frac{1}{2m}\rho S_{ref} C_D = \left(\frac{dV}{ds}\right)_0 \left(\frac{V_0}{V}\right)^n . \tag{38}$$

The retardation shown in equation 38 presents the retardation in terms of a fractional (or percentage if multiplied by 100) loss in velocity per unit length of travel. This form of the retardation is independent of velocity for a constant drag coefficient and perhaps is more appropriate as a parameter characterizing the munition in the subsonic regime where the drag coefficient is relatively constant.

While it is possible to use any of the three definitions of retardation as a means of characterizing munition performance, for the munitions examined here, the drag coefficient exponent was closer to one than zero. The muzzle retardation obtained using equation 20 is less sensitive to velocity than the other two definitions of retardation and is perhaps more representative of the performance of the projectile than the other two definitions. For point designs where the muzzle velocity and muzzle retardation are fixed, this is perhaps a minor point as the trajectory equations can be normalized by any of the three forms of muzzle retardation and the predicted results will be identical. However, when the variation in performance with muzzle velocity is required, it is better to choose the definition of retardation with the least sensitivity to velocity.

The time-range relationships in equations 25–27 can also be expanded in a Taylor's series as shown in equation 39.

$$(t-t_0)=\frac{1}{\left(\frac{dV}{ds}\right)_0}\left\{\left(\frac{dV}{ds}\right)_0\frac{(s_x-s_{x0})}{V_0}-\frac{1}{2}\left[\left(\frac{dV}{ds}\right)_0\frac{(s_x-s_{x0})}{V_0}\right]^2+\right.$$
$$+\frac{1}{6}(1+n)\left[\left(\frac{dV}{ds}\right)_0\frac{(s_x-s_{x0})}{V_0}\right]^3-\frac{1}{24}(1+n)(1+2n)\left[\left(\frac{dV}{ds}\right)_0\frac{(s_x-s_{x0})}{V_0}\right]^4+...$$
$$\left.+\frac{(-1)^{j+1}}{j!}(1+n)(1+2n)...(1+(j-2)n)\left[\left(\frac{dV}{ds}\right)_0\frac{(s_x-s_{x0})}{V_0}\right]^j+...\right\}\quad . \tag{39}$$

Equation 39 shows that first two terms of the expansion are independent of the shape of the drag curve, and the drag coefficient exponent only appears in the cubic and higher-order terms.

Figures 6 and 7 show the scaled time-of-flight as a function of range for various values of the drag coefficient exponent. The time-of-flight is only modestly effected by the drag coefficient variation. For the nominal kinetic energy projectile muzzle velocity and retardation (1600 m/s and 60 [m/s]/km), the time of flight to 5 km is 3.461 s and 3.437 s for a range of exponents that varies from $1/M$ (n = 1) to constant drag coefficient (n = 0). For comparison, the time-of-flight to 5 km is 2.941 s for a hypothetical projectile with zero drag (vacuum trajectory). Thus, the muzzle retardation is seen to have a more important influence on the time-of-flight than the drag coefficient exponent. As seen before, the effect of drag variation is more apparent for rounds with higher retardation such as training ammunition or HEAT rounds. For typical training ammunition (muzzle velocity of 1700 m/s and retardation of 220 [m/s]/km), the time of flight to 2.5 km is 2.039 s and 1.908 s, when drag coefficient varies with $1/M$ (n = 1) or when the drag coefficient is constant (n = 0), respectively. The time of flight is proportionally the same for the nominal HEAT round (muzzle velocity of 1100 m/s and retardation of 340 [m/s]/km), 3.15 s and 2.95 s, although the time of flight longer because of the lower muzzle velocity.

### 3.2 Change in Impact Velocity and Time-of-Flight Due to Change in Muzzle Velocity

The velocity-range relations previously shown (equations 21, 22, and 31) can be used to derive other important relations. For instance, changes in muzzle velocity produce changes in the impact velocity on the target downrange. Whether these changes are produced by design modifications or are part of the experimentally observed muzzle velocity variability observed in the experimental testing, it is important to be able to predict the resulting change in the impact velocity due to changes in muzzle velocity. The velocity-range relations can be used to determine the variation in impact velocities due to changes in muzzle velocity. Using the velocity-range relations in equations 21 and 22, it can be shown that the change in impact velocity with change in muzzle velocity for a fixed range has the form shown in equation 40.

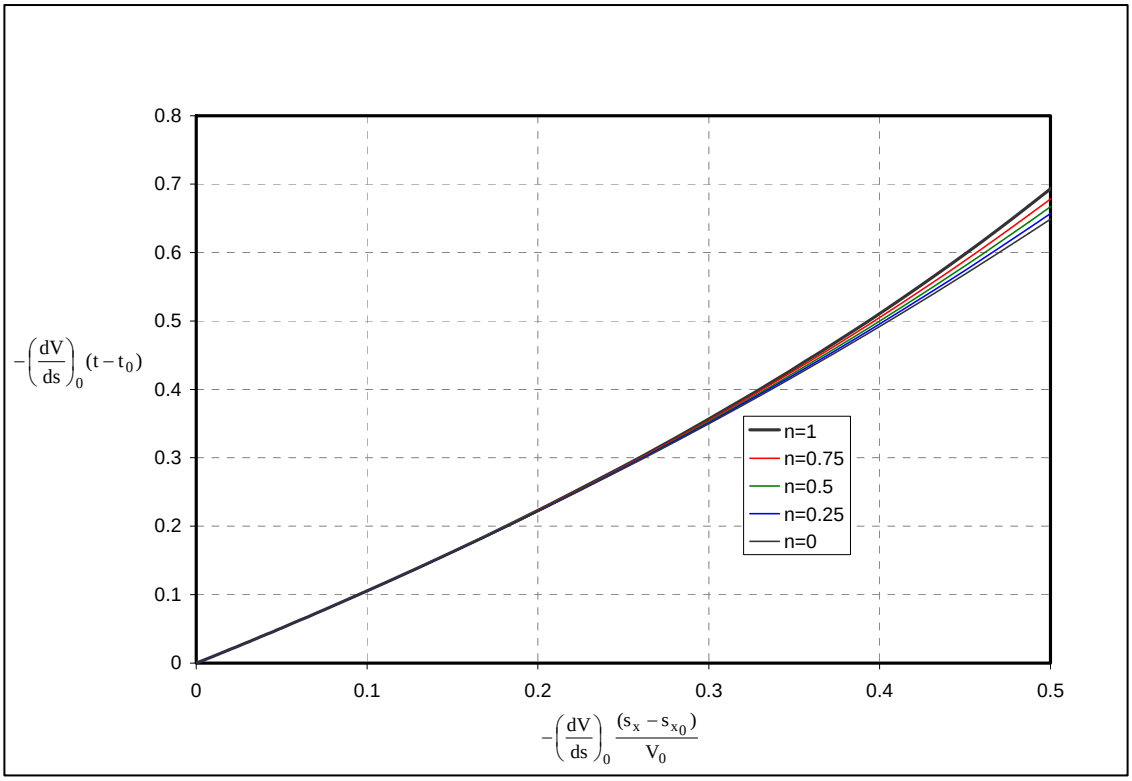


Figure 6. Scaled time-of-flight as a function of scaled range.

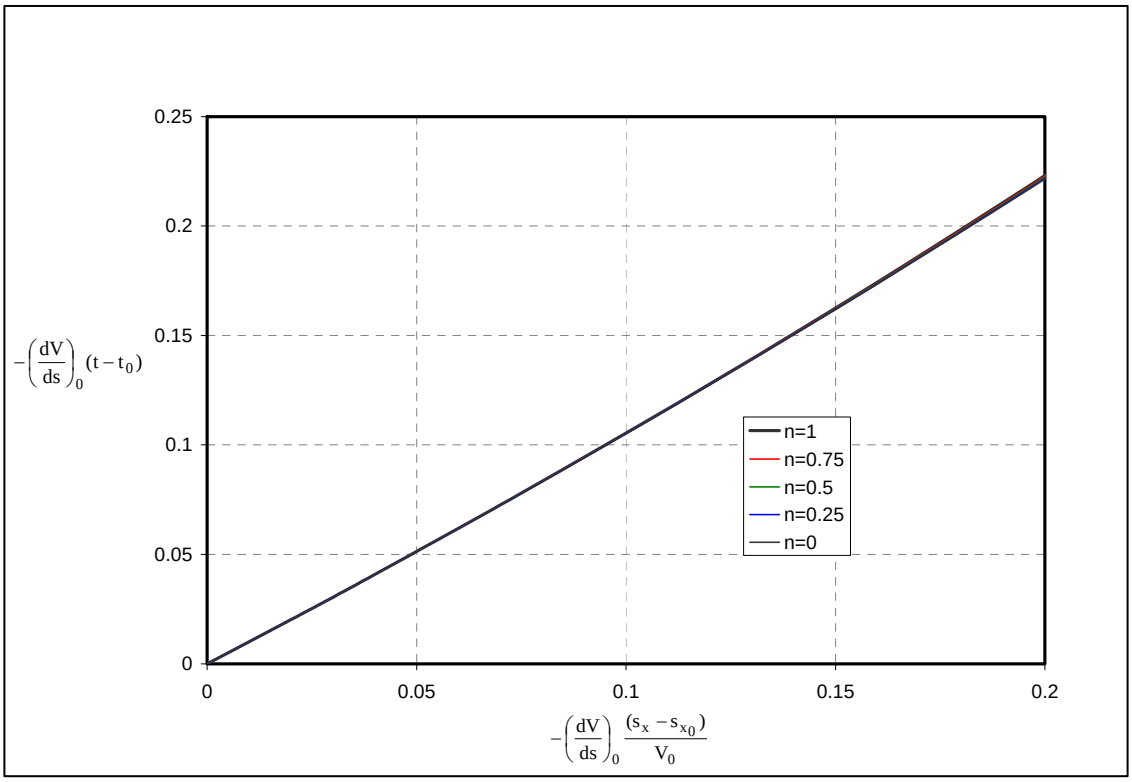


Figure 7. Scaled time-of-flight as a function of scaled range (close-up).

This allows the change in impact velocity with change in muzzle velocity to be easily computed using the existing velocity relationships shown in equations 21 and 22.

$$\frac{dV}{dV_0} = \left(\frac{V}{V_0}\right)^{1-n}. \tag{40}$$

Using the Taylor's series expansion form in equation 31, the variation in impact velocity with changes in muzzle velocity can also be obtained in the form shown in equation 41.

$$\frac{dV}{dV_0} = 1 + (1-n)\left(\frac{dV}{ds}\right)_0 \frac{(s_x - s_{x0})}{V_0} + \frac{1}{2}(1-n)(1-2n)\left\{\left(\frac{dV}{ds}\right)_0 \frac{(s_x - s_{x0})}{V_0}\right\}^2 + \ldots$$
$$+ \frac{1}{j!}(1-n)(1-2n)\ldots(1-(j-1)n)(1-j\cdot n)\left\{\left(\frac{dV}{ds}\right)\frac{(s_x - s_{x0})}{V_0}\right\}^j + \ldots \tag{41}$$

It is noted that this expansion is equivalent to the expansion for the change in retardation with change in range previously shown in equation 33, by virtue of the chain rule for derivatives.

Figure 8 shows the variation in impact velocity with changes in muzzle velocity as a function of scaled range for several values of the drag coefficient exponent. The results show that when the drag varies with the inverse of the Mach number (n = 1), a 1-m/s increase in muzzle velocity produces a 1-m/s increase in impact velocity for all ranges. When the exponent is less than one, changes in muzzle velocity produce slightly less than a one to one change in the impact velocities with the effect increasing with range. For the hypothetical kinetic energy projectile (muzzle velocity of 1600 m/s and a retardation of 60 [m/s]/km), the results show that at 3 km the change in the impact velocity is 94% of the increase in the muzzle velocity for an drag coefficient exponent of 0.5. The change in muzzle velocity drops to 90% at 5 km for the same drag coefficient exponent.

Similarly, the change in time-of-flight due to change in muzzle velocity for a fixed range can be determined using equations 25–27. The form of the solution allows the change in time-of-flight due to change in muzzle velocity easily computed using the existing velocity relationships shown in equations 21 and 22. Although the drag coefficient exponent does not explicitly appear in equation 42, the effect is implicitly included in the velocity variation $V / V_0$.

$$\frac{d(t - t_0)}{dV_0} = \frac{1}{-\left(\frac{dV}{ds}\right)_0 V_0}\left[1 - \left(\frac{V}{V_0}\right)^{-1}\right]. \tag{42}$$

The Taylor's series form for the change in time-of-flight due to change in muzzle velocity can be determined using equation 39 and is shown in equation 43.

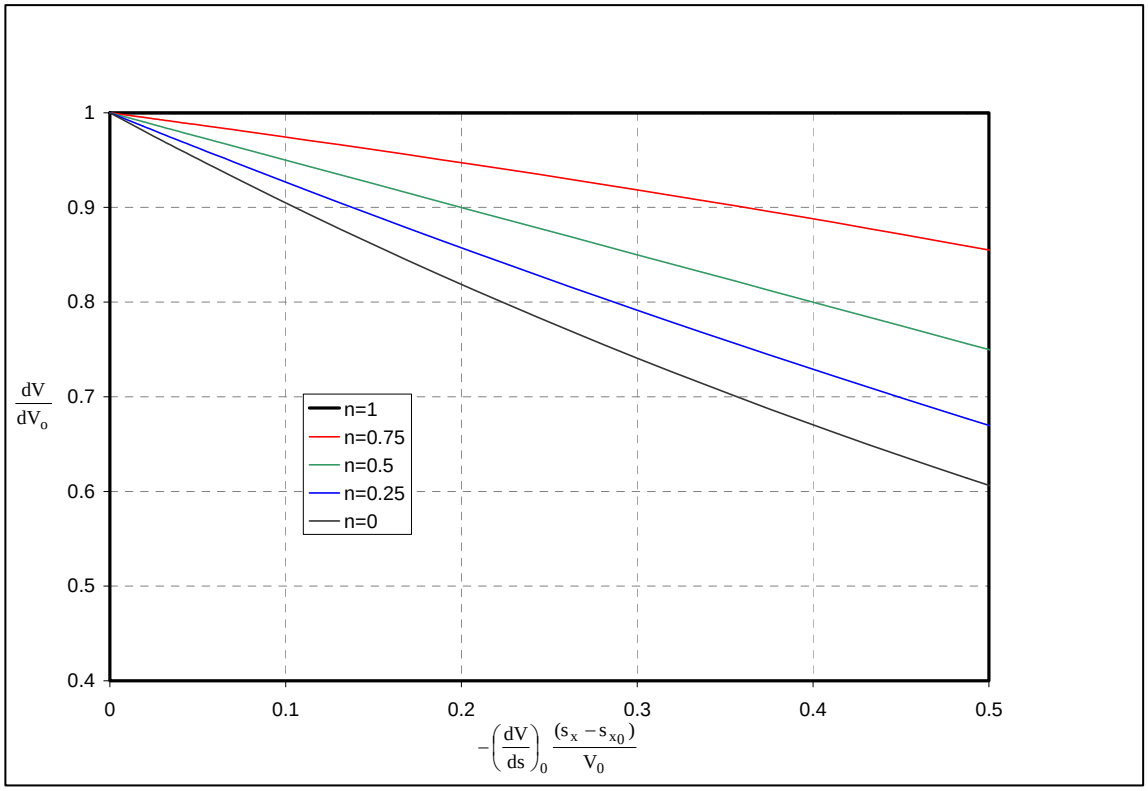


Figure 8. Rate of change of impact velocity with change in muzzle velocity as a function of scaled range.

$$\frac{d(t-t_0)}{dV_0} = \frac{1}{V_0\left(\frac{dV}{ds}\right)_0}\left\{-\left(\frac{dV}{ds}\right)_0\frac{(s_x-s_{x0})}{V_0}+\frac{(1+n)}{2}\left[\left(\frac{dV}{ds}\right)_0\frac{(s_x-s_{x0})}{V_0}\right]^2\right.$$
$$-\frac{1}{6}(1+n)(1+2n)\left[\left(\frac{dV}{ds}\right)_0\frac{(s_x-s_{x0})}{V_0}\right]^3+$$
$$+\frac{1}{24}(1+n)(1+2n)(1+3n)\left[\left(\frac{dV}{ds}\right)_0\frac{(s_x-s_{x0})}{V_0}\right]^4+\ldots$$
$$\left.+\frac{(-1)^j}{j!}(1+n)(1+2n)\ldots(1+(j-1)n)\left[\left(\frac{dV}{ds}\right)_0\frac{(s_x-s_{x0})}{V_0}\right]^j+\ldots\right\}. \qquad (43)$$

Figure 9 shows a plot of the scaled change in time-of-flight with change in muzzle velocity as a function of scaled range. For shorter ranges, the results are relatively independent of the drag coefficient exponent. As shown in equation 43, to leading order, the results are independent of both the drag coefficient exponent and muzzle retardation. Typically, the change in time of flight with change in muzzle velocity is relatively small and by itself is relatively unimportant. However, the change in time of flight due to change in muzzle velocity can have a measurable

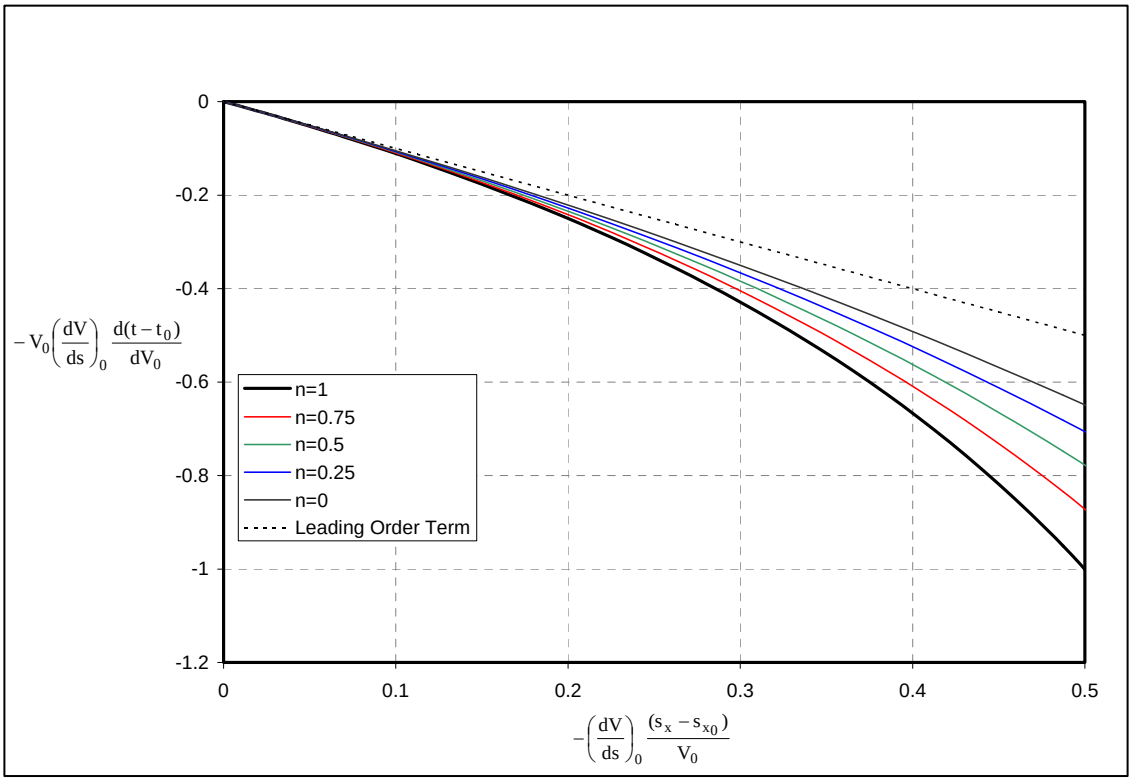


Figure 9. Scaled rate of change of time-of-flight with change in muzzle velocity as a function of scaled range.

impact on the dispersion of the projectile. The effect of the variability of muzzle velocity on impact location is considered in a later section.

### 3.3 Change in Impact Velocity and Time-of-Flight Due to Change in Muzzle Retardation

In a similar manner, changes in the muzzle retardation can have an effect on the impact velocity and time-of-flight for a projectile. Change in the muzzle retardation can result from changes in the atmospheric density, drag coefficient, and mass as seen in equation 20. Changes in the muzzle retardation are also produced by changes in the muzzle velocity, although these effects are implicitly included in the results presented in the previous section. Using the velocity-range relations in equations 21 and 22, it can be shown that the change in impact velocity with change in muzzle retardation for a fixed range has the form shown in equation 44.

$$\frac{dV}{d\left(\frac{dV}{ds}\right)_0} = \frac{V_0}{\left(\frac{dV}{ds}\right)_0}\left(\frac{V}{V_0}\right)^{1-n}\left[\left(\frac{dV}{ds}\right)_0 \frac{(s_x - s_{x0})}{V_0}\right] . \tag{44}$$

A Taylor's series expansion for the change in impact velocity with change in retardation can be found as follows.

$$\frac{dV}{d\left(\frac{dV}{ds}\right)_0} = \frac{V_0}{\left(\frac{dV}{ds}\right)_0}\left\{\left(\frac{dV}{ds}\right)_0 \frac{(s_x - s_{x0})}{V_0} + (1-n)\left\{\left(\frac{dV}{ds}\right)_0 \frac{(s_x - s_{x0})}{V_0}\right\}^2 + \ldots\right.$$

$$\left. + \frac{1}{(j-1)!}(1-n)(1-2n)\ldots(1-(j-2)n)(1-(j-1)n)\left\{\left(\frac{dV}{ds}\right)\frac{(s_x - s_{x0})}{V_0}\right\}^j + \ldots\right\} . \quad (45)$$

The Taylor's series expansion represents the exact solution for n = 1/j where j is a positive non-zero integer. For n = 1, the change in impact velocity with change in muzzle retardation increases linearly with range. This is expected since the velocity history itself varies linearly with range and the retardation is constant when n = 1.

The scaled rate of change of impact velocity with change in retardation as a function of scaled range is shown in figure 10. The results show a linear variation with range for n = 1, with the rate of change of impact velocity decreasing as the drag coefficient exponent decreases.

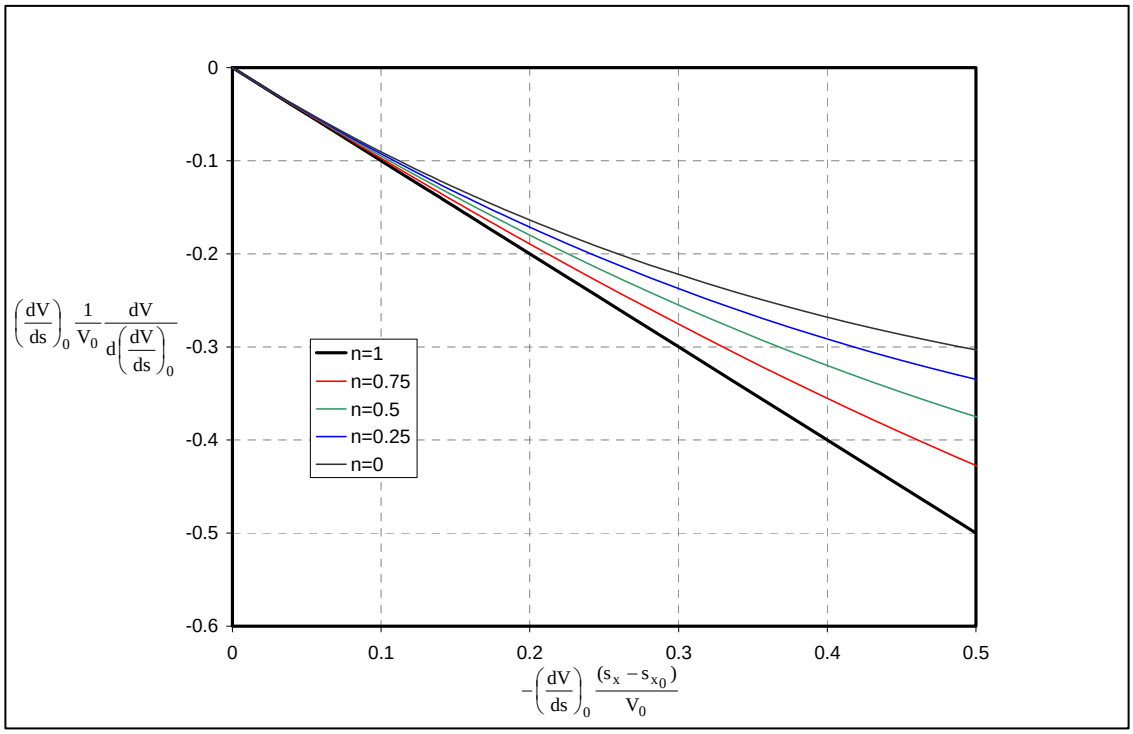


Figure 10. Scaled rate of change of impact velocity with change in muzzle retardation as a function of scaled range.

Similarly, the change in time-of-flight with change in muzzle retardation for a fixed range can be derived and has the form shown in equation 46.

$$\frac{d(t-t_0)}{d\left(\frac{dV}{ds}\right)_0} = \frac{1}{\left(\frac{dV}{ds}\right)_0^2}\left\{-\left(\frac{dV}{ds}\right)_0 (t-t_0) + \left(\frac{V}{V_0}\right)^{-1}\left[\left(\frac{dV}{ds}\right)_0 \frac{(s_x - s_{x0})}{V_0}\right]\right\}. \tag{46}$$

A Taylor's series expansion for the change in time of flight with change in retardation can be found as shown in equation 47.

$$\begin{aligned}\frac{d(t-t_0)}{d\left(\frac{dV}{ds}\right)_0} = \frac{1}{\left(\frac{dV}{ds}\right)_0^2}\Bigg\{ & -\frac{1}{2}\left[\left(\frac{dV}{ds}\right)_0 \frac{(s_x - s_{x0})}{V_0}\right]^2 \\ & + \frac{1}{3}(1+n)\left[\left(\frac{dV}{ds}\right)_0 \frac{(s_x - s_{x0})}{V_0}\right]^3 + \\ & - \frac{1}{8}(1+n)(1+2n)\left[\left(\frac{dV}{ds}\right)_0 \frac{(s_x - s_{x0})}{V_0}\right]^4 + \ldots \\ & + \frac{(j-1)(-1)^{j+1}}{j!}(1+n)(1+2n)\ldots(1+(j-2)n)\left[\left(\frac{dV}{ds}\right)_0 \frac{(s_x - s_{x0})}{V_0}\right]^j + \ldots\Bigg\}.\end{aligned} \tag{47}$$

Figure 11 shows the scaled rate of change of time-of-flight with change in muzzle retardation as a function of scaled range. The largest change is observed when the drag coefficient exponent is the largest.

## 4. Solution of the 2-DOF Equations

The 1-DOF point-mass equations provide useful information about the flight behavior of direct-fire munitions. However, there are aspects of the flight trajectory that require the vertical equation of motion and the effect of gravity to be considered. In this case, the 2-DOF equations, shown previously in equations 1–4, must be solved. Exact analytical solution of the 2-DOF equations can be obtained when the drag coefficient varies with the inverse of the Mach number (n = 1 variation as previously shown in equation 10). In this case, the coefficients in equations 1 and 2 are constant, as shown in equations 48 and 49, and the governing equations are a set of first order linear ordinary differential equations with constant coefficients.

$$\frac{dV_x}{dt} - \left(\frac{dV}{ds}\right)_0 V_x = 0. \tag{48}$$

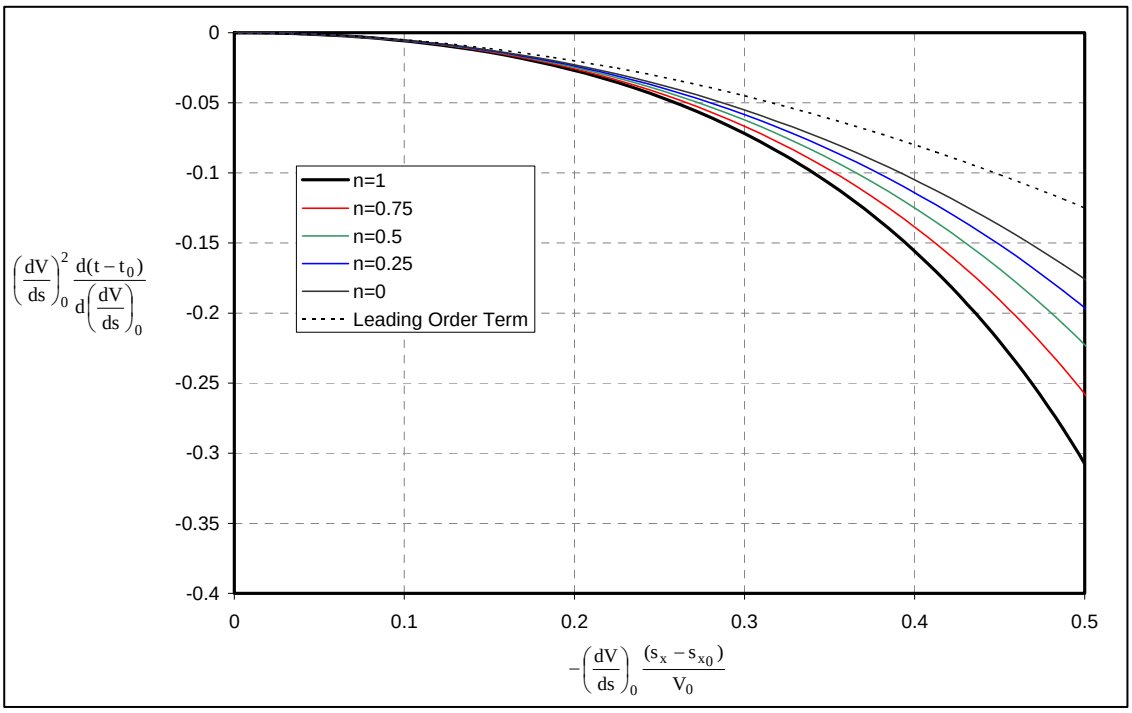


Figure 11. Scaled rate of change of time-of-flight with change in muzzle retardation as a function of scaled range.

$$\frac{dV_y}{dt} - \left(\frac{dV}{ds}\right)_0 V_y = -g\,. \tag{49}$$

$$\frac{ds_x}{dt} = V_x\,. \tag{50}$$

$$\frac{ds_y}{dt} = V_y\,. \tag{51}$$

The solution is shown below. The solution is composed of the homogeneous solution that consists of the 1-DOF solution resolved in the *x*- and *y*-directions plus the particular solution which includes the effect of gravity on the trajectory.

$$V_x = \overline{V}\cos\theta_0\,. \tag{52}$$

$$V_y = \overline{V}\sin\theta_0 + V_y^P\,. \tag{53}$$

$$s_x - s_{x0} = \bar{s}\cos\theta_0\,. \tag{54}$$

$$s_y - s_{y0} = \bar{s}\sin\theta_0 + s_y^P\,. \tag{55}$$

$$\overline{V} = V_0 \exp\left\{\left(\frac{dV}{ds}\right)_0 (t - t_0)\right\}\,. \tag{56}$$

$$\bar{s} = \frac{V_0}{-\left(\frac{dV}{ds}\right)_0}\left(1-\exp\left\{\left(\frac{dV}{ds}\right)_0 (t-t_0)\right\}\right). \tag{57}$$

$$V_y^P = +\frac{g}{\left(\frac{dV}{ds}\right)_0}\left(1-\exp\left\{\left(\frac{dV}{ds}\right)_0 (t-t_0)\right\}\right). \tag{58}$$

$$s_y^P = +\frac{g}{\left(\frac{dV}{ds}\right)_0^2}\left(1+\left(\frac{dV}{ds}\right)_0 (t-t_0) - \exp\left\{\left(\frac{dV}{ds}\right)_0 (t-t_0)\right\}\right) \equiv s_{g-drop}. \tag{59}$$

The particular solution for the vertical displacement, equation 59, represent the downward deflection in the trajectory due to gravity or "gravity drop."

For direct-fire applications, approximate (but very accurate) solutions to the 2-DOF equations can be obtained when the drag coefficient has the variation shown in equation 10. In this case, equations 1 and 2 can be rewritten as shown in equations 60 and 61.

$$\frac{dV_x}{dt} - \left(\frac{dV}{ds}\right)_0 \left(\frac{V}{V_0}\right)^{1-n} V_x = 0. \tag{60}$$

$$\frac{dV_y}{dt} - \left(\frac{dV}{ds}\right)_0 \left(\frac{V}{V_0}\right)^{1-n} V_y = -g. \tag{61}$$

These equations are nonlinear and coupled. Within the constraints of the approximations that were previously made for direct-fire munitions, the velocity variation in the coefficients of equations 60 and 61 can actually be expressed as a function of time using the results from the solution of the 1-DOF equation (equation 23).

$$\left(\frac{V}{V_0}\right)^{n-1} = 1+(n-1)\left(\frac{dV}{ds}\right)_0 (t-t_0). \tag{62}$$

$$\left\{1+(n-1)\left(\frac{dV}{ds}\right)_0 (t-t_0)\right\}\frac{dV_x}{dt} - \left(\frac{dV}{ds}\right)_0 V_x = 0. \tag{63}$$

$$\left\{1+(n-1)\left(\frac{dV}{ds}\right)_0 (t-t_0)\right\}\frac{dV_y}{dt} - \left(\frac{dV}{ds}\right)_0 V_y = -g\left\{1+(n-1)\left(\frac{dV}{ds}\right)_0 (t-t_0)\right\}. \tag{64}$$

Essentially, this assumes that the contribution from gravity in the total velocity can be ignored. This uncouples the equations and effectively makes the equations linear, although the coefficients are functions of time. Because the equations are linear, solutions for the equations

can be obtained by seeking the homogeneous and particular solutions of the ordinary differential equations. The solution has the same form as equations 52–55, and the expressions for $\bar{s}$, $\overline{V}$, $s_y^P$, and $V_y^P$ are shown in equations 65–72 for various values of the drag coefficient exponent n.

$$\overline{V} = V_0\left\{1+(n-1)\left(\frac{dV}{ds}\right)_0 (t-t_0)\right\}^{\frac{1}{n-1}} \qquad n \neq 1. \tag{65}$$

$$\bar{s} = \frac{V_0}{-\left(\frac{dV}{ds}\right)_0 n}\left[1-\left\{1+(n-1)\left(\frac{dV}{ds}\right)_0 (t-t_0)\right\}^{\frac{n}{n-1}}\right] \qquad n \neq 1, n \neq 0. \tag{66}$$

$$\bar{s} = \frac{V_0}{-\left(\frac{dV}{ds}\right)_0}\ln\left\{1-\left(\frac{dV}{ds}\right)_0 (t-t_0)\right\} \qquad n = 0. \tag{67}$$

$$V_y^P = \frac{g}{(n-2)\left(\frac{dV}{ds}\right)_0}\left[\left\{1+(n-1)\left(\frac{dV}{ds}\right)_0 (t-t_0)\right\}^{\frac{1}{n-1}} - \left\{1+(n-1)\left(\frac{dV}{ds}\right)_0 (t-t_0)\right\}\right] \qquad n \neq 1, 2\ . \tag{68}$$

$$V_y^P = \frac{-g}{\left(\frac{dV}{ds}\right)_0}\left\{1+\left(\frac{dV}{ds}\right)_0 (t-t_0)\right\}\ln\left\{1+\left(\frac{dV}{ds}\right)_0 (t-t_0)\right\} \qquad n = 2\ . \tag{69}$$

$$s_y^P = \frac{-g}{2\left(\frac{dV}{ds}\right)_0^2}\left\{\frac{1}{2}\left(\frac{dV}{ds}\right)_0^2 (t-t_0)^2 - \left(\frac{dV}{ds}\right)_0 (t-t_0) - \ln\left(1-\left(\frac{dV}{ds}\right)_0 (t-t_0)\right)\right\} \qquad n = 0\ . \tag{70}$$

$$s_y^P = \frac{-g}{2\left(\frac{dV}{ds}\right)_0^2}\left[\left\{1+\left(\frac{dV}{ds}\right)_0 (t-t_0)\right\}^2 \ln\left\{1+\left(\frac{dV}{ds}\right)_0 (t-t_0)\right\} - \left(\frac{dV}{ds}\right)_0 (t-t_0) - \frac{1}{2}\left(\frac{dV}{ds}\right)_0^2 (t-t_0)^2\right] \qquad n = 2\ . \tag{71}$$

$$s_y^P = \frac{-g}{n(n-2)\left(\frac{dV}{ds}\right)_0^2}\left[1+n\left(\frac{dV}{ds}\right)_0(t-t_0)+\frac{n(n-1)}{2}\left(\frac{dV}{ds}\right)_0^2(t-t_0)^2 - \left\{1+(n-1)\left(\frac{dV}{ds}\right)_0(t-t_0)\right\}^{\frac{n}{n-1}}\right] \quad n \neq 0, n \neq 1, n \neq 2 \ . \tag{72}$$

Here, solutions for various values of the drag coefficient exponent are presented. The solutions for n = 2 are included for completeness, although this value of the drag coefficient exponent is larger than the drag coefficient exponents examined here. Again, the solution of the 2-DOF equations can be characterized as the 1-DOF solution resolved in the *x* and *y* directions (homogeneous solution) plus the gravity drop term (particular solution).

In the previous equations, solutions have been determined as a function of the time-of-flight. Using these solutions, it is also possible to obtain solutions as a function of range by inverting the expressions for range as a function of time-of-flight. From equation 54,

$$\bar{s} = \frac{s_x - s_{x_0}}{\cos\theta_0}. \tag{73}$$

For flat fire, the angle $\theta_0$ is small and $\cos\theta_0 \cong 1$.

$$\bar{s} \cong s_x - s_{x_0}. \tag{74}$$

The approximation shown in equation 74 removes the dependency of the two range coordinates on the angle of elevation. This is an important approximation because, when the 2-DOF equations are inverted, many of the resulting expressions as a function of range become independent of gun elevation angle. The exact expression in equation 73 can be retained without too much additional complexity in the resulting expressions. However, the implicit dependence of the gun elevation angle within the resulting expressions appears unnecessary for the applications examined here and the approximation is equation 74 is utilized in the remaining analysis.

Using equation 74 and equations 57, 66, and 67 can inverted to obtain expressions of the time-of-flight as a function of range which are essentially equivalent to equations 25–27.

$$(t-t_0) = \frac{1}{(n-1)\left(\frac{dV}{ds}\right)_0}\left[\left\{1+n\left(\frac{dV}{ds}\right)_0\frac{(s_x - s_{x_0})}{V_0}\right\}^{1-\frac{1}{n}} - 1\right] \quad n \neq 0, n \neq 1 \ . \tag{75}$$

$$(t - t_0) = \frac{1}{\left(\frac{dV}{ds}\right)_0} \ln\left\{1 + \left(\frac{dV}{ds}\right)_0 \frac{(s_x - s_{x0})}{V_0}\right\} \quad n = 1 \ . \tag{76}$$

$$(t - t_0) = \frac{1}{\left(\frac{dV}{ds}\right)_0} \left[1 - \exp\left\{-\left(\frac{dV}{ds}\right)_0 \frac{(s_x - s_{x0})}{V_0}\right\}\right] \quad n = 0 \ . \tag{77}$$

Equation 73 can be combined with equation 55 to obtain an expression for the vertical displacement along the trajectory as a function of range.

$$s_y - s_{y0} = (s_x - s_{x0}) \tan\theta_0 + s_y^P \ . \tag{78}$$

Using equations 75–77, the particular solution $s_y^P$ (or gravity drop) can written in term of range instead of time-of-flight.

$$s_y^P = \frac{g}{\left(\frac{dV}{ds}\right)_0^2} \left( -\left(\frac{dV}{ds}\right)_0 \frac{(s_x - s_{x0})}{V_0} + \ln\left\{1 + \left(\frac{dV}{ds}\right)_0 \frac{(s_x - s_{x0})}{V_0}\right\}\right) \qquad n = 1 \ . \tag{79}$$

$$s_y^P = \frac{-g}{4\left(\frac{dV}{ds}\right)_0^2} \left( 2\left(\frac{dV}{ds}\right)_0 \frac{(s_x - s_{x0})}{V_0} + \exp\left\{-2\left(\frac{dV}{ds}\right)_0 \frac{(s_x - s_{x0})}{V_0}\right\} - 1\right) \qquad n = 0 \ . \tag{80}$$

$$s_y^P = \frac{-g}{4\left(\frac{dV}{ds}\right)_0^2} \left[ \left(1 + 2\left(\frac{dV}{ds}\right)_0 \frac{(s_x - s_{x0})}{V_0}\right) \ln\left(1 + 2\left(\frac{dV}{ds}\right)_0 \frac{(s_x - s_{x0})}{V_0}\right) - 2\left(\frac{dV}{ds}\right)_0 \frac{(s_x - s_{x0})}{V_0} \right] \qquad n = 2 \ . \tag{81}$$

$$s_y^P = \frac{-g}{2(n-2)(n-1)\left(\frac{dV}{ds}\right)_0^2} \left[ \left\{1 + n\left(\frac{dV}{ds}\right)_0 \frac{(s_x - s_{x0})}{V_0}\right\}^{\frac{2(n-1)}{n}} - 1 - 2(n-1)\left(\frac{dV}{ds}\right)_0 \frac{(s_x - s_{x0})}{V_0} \right] \qquad n \neq 0,1,2 \ . \tag{82}$$

Similarly, expressions for $V_x$ and $V_y$ can be written in terms of range by expressing $\overline{V}$ and $V_y^P$ as functions of range using equations 75–77.

$$V_x = \overline{V}\cos\theta_0 \ , \tag{83}$$

$$V_y = \overline{V}\sin\theta_0 + V_y^P \ , \tag{84}$$

where

$$\overline{V} = V_0\left\{1 + n\left(\frac{dV}{ds}\right)_0 \frac{(s_x - s_{x0})}{V_0}\right\}^{\frac{1}{n}} \quad n \neq 0 \ , \tag{85}$$

$$\overline{V} = V_0 \exp\left\{\left(\frac{dV}{ds}\right)_0 \frac{(s_x - s_{x0})}{V_0}\right\} \quad n = 0 \ , \tag{86}$$

$$V_y^P = \frac{-g}{\left(\frac{dV}{ds}\right)_0}\left(\left(\frac{dV}{ds}\right)_0 \frac{(s_x - s_{x0})}{V_0}\right) \qquad n = 1 \ , \tag{87}$$

$$V_y^P = \frac{-g}{2\left(\frac{dV}{ds}\right)_0}\left[\exp\left(\left(\frac{dV}{ds}\right)_0 \frac{(s_x - s_{x0})}{V_0}\right) - \exp\left(-\left(\frac{dV}{ds}\right)_0 \frac{(s_x - s_{x0})}{V_0}\right)\right] \qquad n = 0 \ , \tag{88}$$

$$V_y^P = \frac{-g}{2\left(\frac{dV}{ds}\right)_0}\left[\left(1 + 2\left(\frac{dV}{ds}\right)_0 \frac{(s_x - s_{x0})}{V_0}\right)^{1/2} \ln\left(1 + 2\left(\frac{dV}{ds}\right)_0 \frac{(s_x - s_{x0})}{V_0}\right)\right] \qquad n = 2 \ , \tag{89}$$

and

$$V_y^P = \frac{-g}{(n-2)\left(\frac{dV}{ds}\right)_0}\left[\left\{1 + n\left(\frac{dV}{ds}\right)_0 \frac{(s_x - s_{x_0})}{V_0}\right\}^{\frac{n-1}{n}}, \right.$$
$$\left. - \left\{1 + n\left(\frac{dV}{ds}\right)_0 \frac{(s_x - s_{x_0})}{V_0}\right\}^{\frac{1}{n}}\right] \qquad n \neq 0,1,2 \quad . \tag{90}$$

Alternatively, it is also possible to obtain solutions by integrating the equations of motions with range as the independent variable. The solution has the same form as the results just presented.

The vertical velocity component due to gravity (equations 87–90) can be compared with the total velocity in the absence of the gravity (equations 85 and 86). Figure 12 shows the two velocity components as a function of the scaled range. The vertical velocity due to gravity is shown for a fixed value of the gravitational scaling factor of –0.102. This value corresponds to the

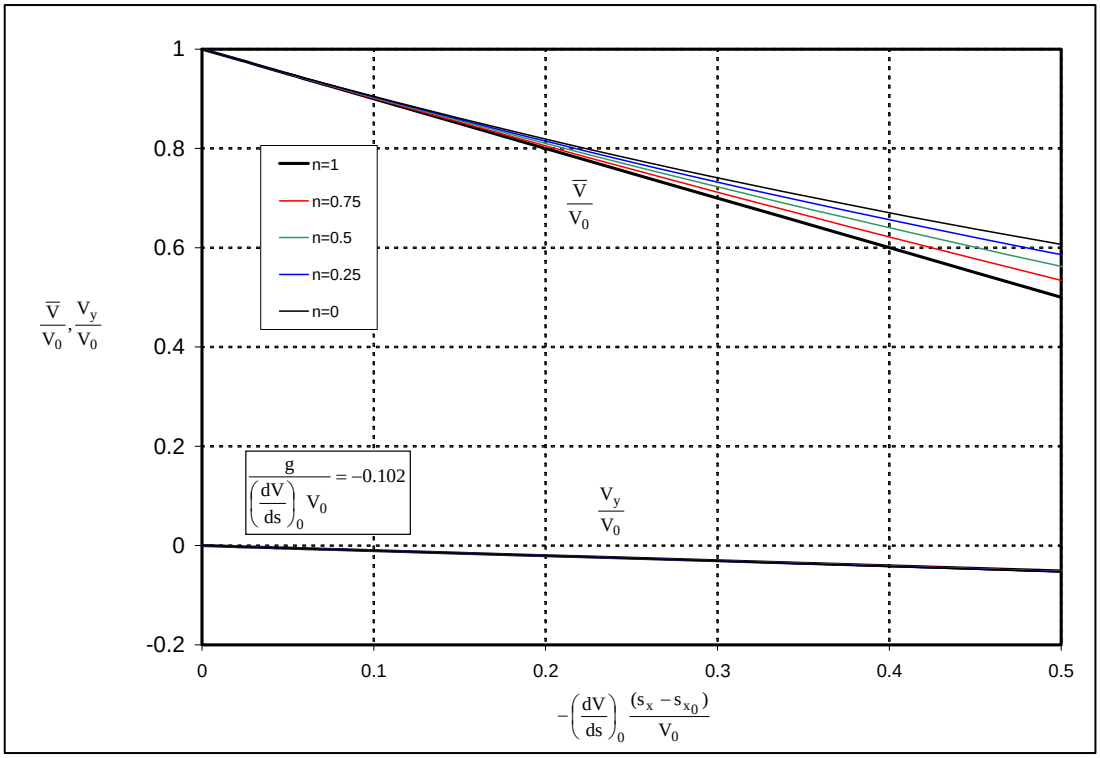


Figure 12. Comparison of the total velocity in the absence of gravity with the vertical velocity due to gravity as a function of scaled range.

gravitational scaling factor for a notional kinetic-energy (KE) projectile with a muzzle velocity of 1600 m/s and a retardation of $-60$ (m/s)/km. The vertical velocity is less than 10% of the total velocity in the absence of gravity even to very large ranges displayed here. For zero gun elevation angle, the square root of the sum of the squares of the horizontal and vertical velocity components shows that the contribution of the vertical velocity due to gravity to the total velocity is less than a half of a percent. The results justify the assumption of ignoring the velocity component due to gravity when evaluating the coefficients of equations 60 and 61. The gravity effect shown in figure 12 is relatively large for the munitions of interest here. For the notational HEAT and training rounds previously discussed, the expected vertical velocity due to gravity is 2.5 to 6 times less than for that shown in figure 12.

The particular solutions for the vertical displacement as a function of time (equations 59 and 70–72) represent the downward deflection in the trajectory due to gravity or "gravity drop." The gravity drop term can be expanded in a Taylor's series as shown in equation 91.

$$s_{g-drop} = -g\left(\frac{1}{2}(t-t_0)^2 + \frac{1}{6}\left(\frac{dV}{ds}\right)_0 (t-t_0)^3 - \frac{1}{24}\left(\frac{dV}{ds}\right)_0^2 (2n-3)(t-t_0)^4 + \frac{1}{120}\left(\frac{dV}{ds}\right)_0^3 (2n-3)(3n-4)(t-t_0)^5 - \frac{1}{720}\left(\frac{dV}{ds}\right)_0^4 (2n-3)(3n-4)(4n-5)(t-t_0)^6 + \ldots\right) . \quad (91)$$

The expansion is valid for all values of n including n = 1. The leading order term is the deflection due to the gravitation effect of a body in a vacuum $(-1/2\,gt^2)$. There are additional higher-order terms in the gravity drop which account for the drag effect. The drag coefficient exponent appears in the fourth order and higher terms of the expansion.

Figure 13 shows the gravity drop as a function of scaled time-of-flight. The gravity drop increases with increasing time-of-flight. The results show that the gravity drop is relatively insensitive to the value of the drag coefficient exponent. The results also show that the gravity drop can be well approximated within the range of interest using the first two terms of equation 91 (as shown in equation 92). (This is the exact solution for n = 1.5.) This form of the gravity drop includes both the gravity drop in vacuum as well as the first-order retardation effect.

$$s_{g-drop} \cong -g\left(\frac{1}{2}(t-t_0)^2 + \frac{1}{6}\left(\frac{dV}{ds}\right)_0 (t-t_0)^3\right) . \qquad (92)$$

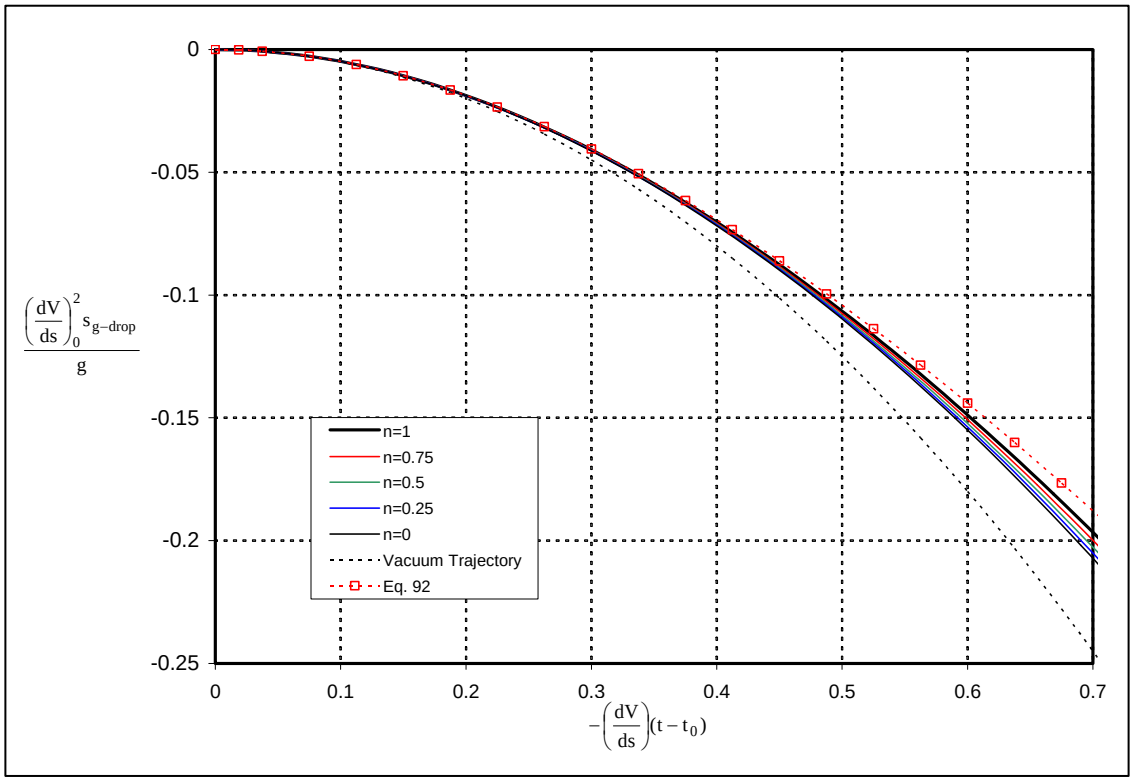


Figure 13. Gravity drop as a function of scaled time-of-flight.

The gravity drop as a function of range can also be expanded in a Taylor's series as shown in equation 93.

$$s_{g-drop} \cong -\frac{g}{\left(\frac{dV}{ds}\right)_0^2}\left\{\frac{1}{2}\left[\left(\frac{dV}{ds}\right)_0 \frac{(s_x - s_{x0})}{V_0}\right]^2 - \frac{1}{3}\left[\left(\frac{dV}{ds}\right)_0 \frac{(s_x - s_{x0})}{V_0}\right]^3 \right.$$
$$+ \frac{(n+2)}{12}\left[\left(\frac{dV}{ds}\right)_0 \frac{(s_x - s_{x0})}{V_0}\right]^4 - \frac{(n+1)(n+2)}{30}\left[\left(\frac{dV}{ds}\right)_0 \frac{(s_x - s_{x0})}{V_0}\right]^5$$
$$\left. + \frac{(-1)^j (n+2)(n+1)(-2)(n+2)(2n+2)...((j-3)n+2)}{j!}\left[\left(\frac{dV}{ds}\right)_0 \frac{(s_x - s_{x0})}{V_0}\right]^j + ...\right\} . \quad (93)$$

The first term of the expansion represents the vacuum trajectory result. The second term includes the lowest-order corrections from the cubic term of equation 91, as well as from longer time-of-flight produced by the retardation effect. Equation 93 shows that the drag coefficient exponent is a higher-order term in the expansion as a function of range.

Figures 14 and 15 show the gravity drop as a function of scaled range. The gravity drop increases with increasing range and the results are relatively insensitive to the value of the drag coefficient exponent. For short ranges, the gravity drop can be well represented by the first two terms of equation 93 (as shown in equation 94).

$$s_{g-drop} \cong -\frac{g}{\left(\frac{dV}{ds}\right)_0^2}\left\{\frac{1}{2}\left[\left(\frac{dV}{ds}\right)_0 \frac{(s_x - s_{x0})}{V_0}\right]^2 - \frac{1}{3}\left[\left(\frac{dV}{ds}\right)_0 \frac{(s_x - s_{x0})}{V_0}\right]^3\right\} . \quad (94)$$

In many direct-fire ballistic applications (jump tests as part of KE projectile accuracy testing is one example), the gravity drop is estimated using the gravity drop in vacuum (the first terms of equations 91 or 93). The results shown here demonstrate that with little additional effort, this estimate can be improved, in some cases significantly, using equations 92 or 94, provided the muzzle retardation of the round is known. If the drag coefficient exponent is known, these estimates can be further improved using additional terms of the expansions or the exact solution.

The solutions of the 2-DOF equations can also be used to predict the gun elevation angle $\theta_0$ required to reach a target at range. Equation 78 can rearranged to yield an expression for the gun elevation angle $\theta_0$. Knowing the vertical and horizontal displacement of the target from the gun and the gravity drop as a function of range (equations 79–82), equation 95 can be solved to determine the gun elevation angle.

$$\tan\theta_0 = \frac{s_y - s_{y0} - s_{g-drop}}{s_x - s_{x0}} . \quad (95)$$

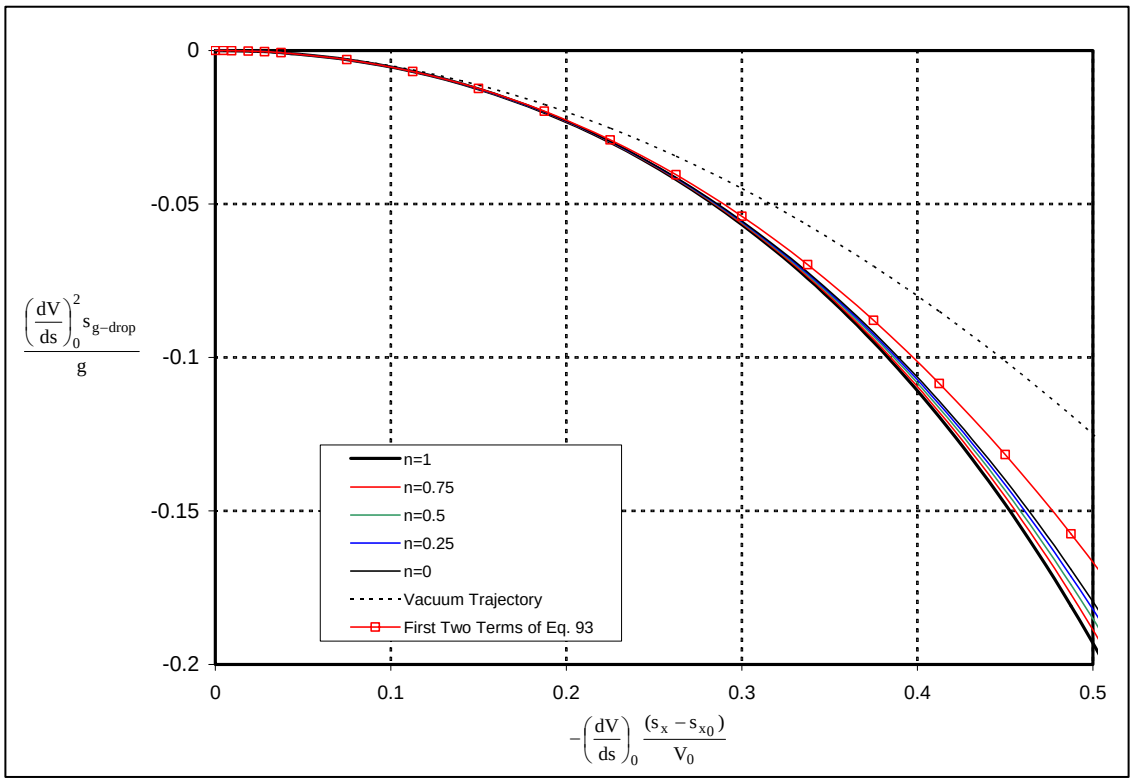


Figure 14. Gravity drop as a function of scaled range.

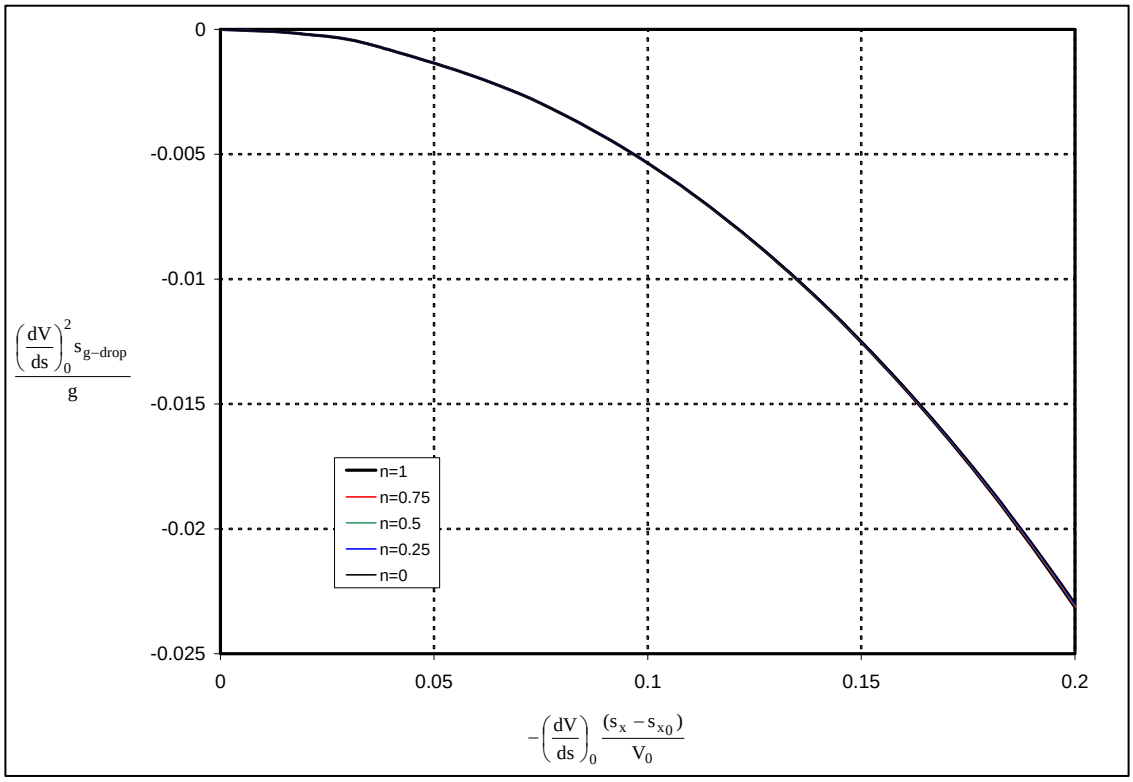


Figure 15. Gravity drop as a function of scaled range (close-up).

Figure 16 shows the predicted gun elevation angle as a function of the scaled range when the target is at the same vertical location as the gun. The gun elevation angle is independent of the drag coefficient exponent at shorter ranges. Also shown is the firing tables data for the M829, M865, and M830 projectiles for ranges to 3 km. The predicted results are consistent with the firing table data for these rounds. The results imply that the gun elevation angle can be predicted for a significant portion of the useful range using only the projectile muzzle velocity and muzzle retardation because the drag coefficient exponent has little influence. Also shown are the results obtained assuming a vacuum trajectory. The vacuum trajectory results are a limiting case at short range, however, by including the retardation effect, the gun elevation angle can be predicted with better accuracy to longer ranges than using the vacuum trajectory.

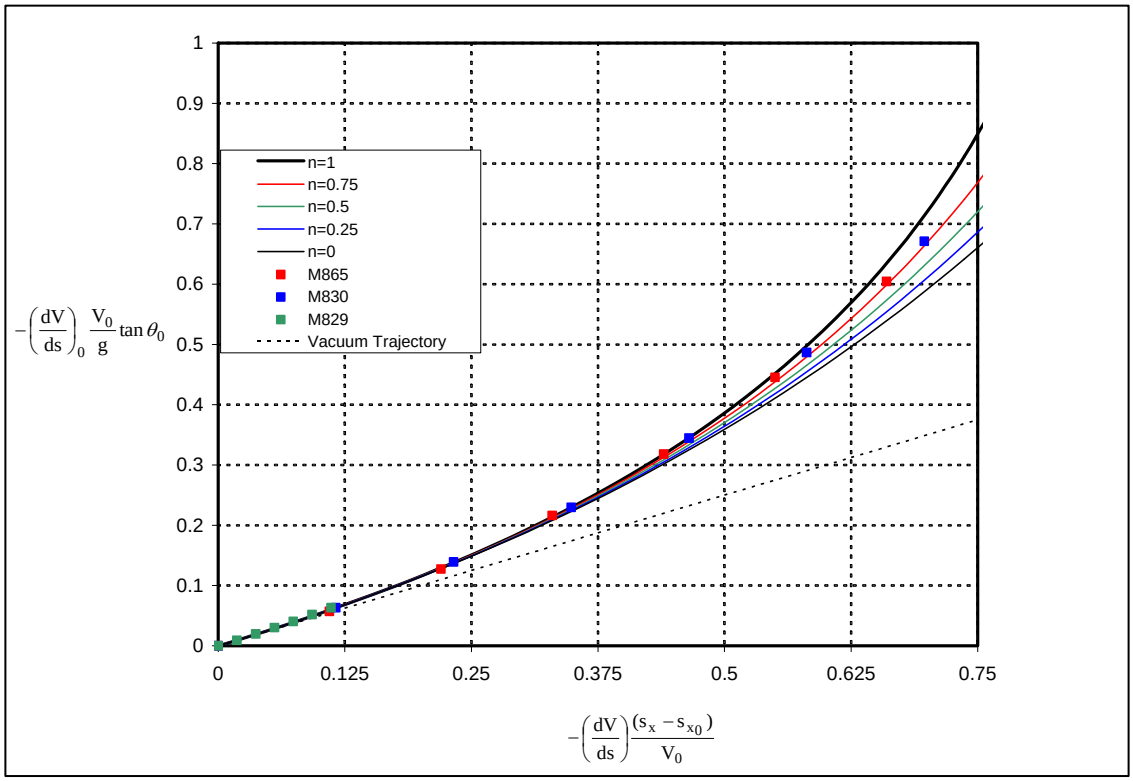


Figure 16. Scaled gun elevation as a function of scaled range.

The angle of inclination of the trajectory at impact can also be determined using the current analysis. This angle can be important for terminal guidance and terminal ballistic effects as well as for determining the variability of the vertical impact location due to errors in estimating range to target. Using equation 78, the slope of the trajectory at impact can be determined from the derivative with respect to range as shown in equation 96.

$$\tan\theta_I = \frac{d(s_y - s_{y_0})}{d(s_x - s_{x_0})} = \tan\theta_0 + \frac{d s_y^P}{d(s_x - s_{x_0})} \ . \qquad (96)$$

By virtue of the chain rule, the last term of equation 96 can be evaluated as shown in equation 97.

$$\frac{ds_y^P}{d(s_x - s_{x_0})} = \frac{V_y^P}{V_x} = \frac{V_y^P}{\overline{V}\cos\theta_0} \quad . \tag{97}$$

Applying the small angle approximation $\cos\theta_0 \cong 1$ to equation 97 yields equation 98.

$$\tan\theta_I = \tan\theta_0 + \frac{V_y^P}{\overline{V}} \quad . \tag{98}$$

Figure 17 shows the predicted trajectory impact angle as a function of the scaled range when the target is at the same vertical location as the gun. For shorter ranges, the trajectory impact angle is independent of the drag coefficient exponent and is nearly equal to the gun elevation angle consistent with the classical vacuum trajectory result. As the range increases, both the trajectory impact angle and the difference between the gun elevation angle and the trajectory impact angle increase.

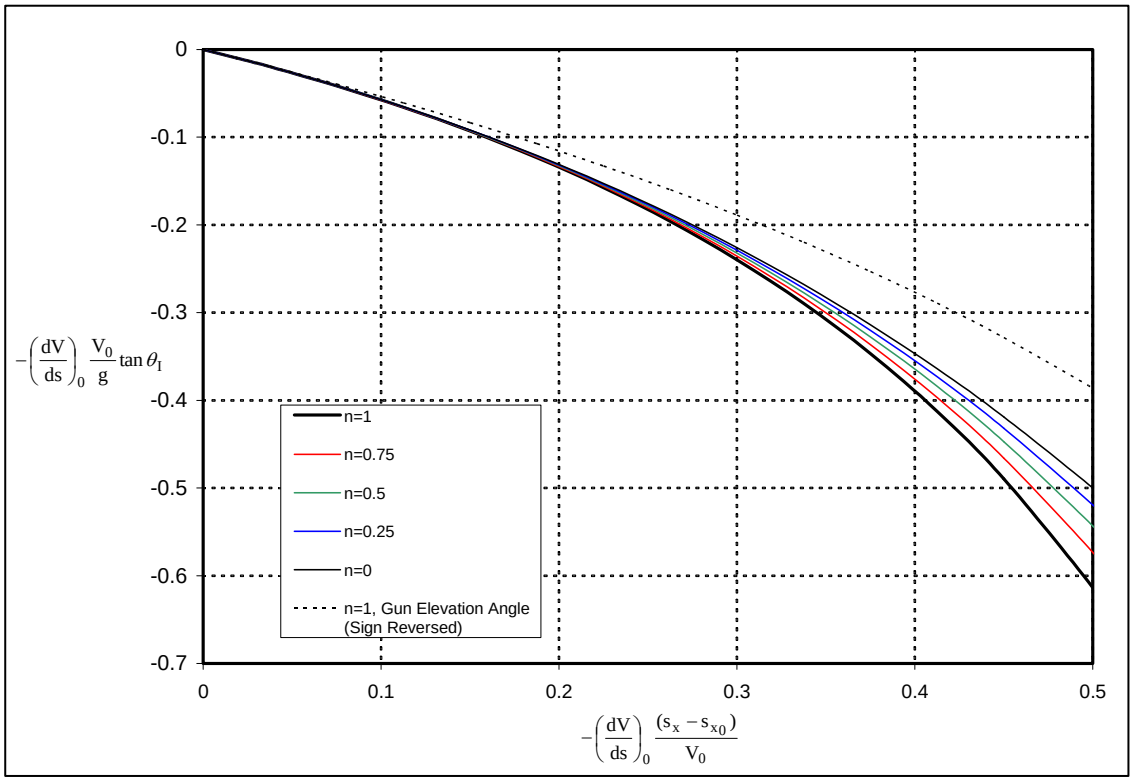


Figure 17. Scaled trajectory impact angle for flat fire as a function of scaled range.

### 4.1 Change in Impact Location Due to Variability in Muzzle Velocity and Muzzle Retardation

As previously discussed, variability in the muzzle velocity and muzzle retardation (typically through variability in the drag coefficient) can have a measurable effect on the impact dispersion of the projectile. These effects are typically manifested through the change in time of flight. The 2-DOF equations can be used to quantify these effects. Typically, the variation of the vertical impact location is desired at a fixed range and gun elevation angle. In this case, the equation 78 provides a convenient form to work with. The variation in vertical impact location with change in muzzle velocity or muzzle retardation can be determined analytically by taking derivatives of the vertical impact location with respect to muzzle velocity or muzzle retardation. Here, only the gravity drop term in equation 78 needs to be considered since the gun elevation and range are assumed constant. To obtain the variation in these quantities for a fixed range, the gravity drop as a function of range (equations 79–82) should be used to obtain the proper derivatives.

$$\frac{d(s_y - s_{y0})}{dV_0} = \frac{ds_{g-drop}}{dV_0} \quad . \tag{99}$$

$$\frac{d(s_y - s_{y0})}{d\left(\frac{dV}{ds}\right)_0} = \frac{ds_{g-drop}}{d\left(\frac{dV}{ds}\right)_0} \quad . \tag{100}$$

These derivatives have been computed and are shown in the appendix.

An alternative approach for predicting the variability of the impact location with muzzle velocity or muzzle retardation is to perform discrete computations for the different values of the muzzle retardation or muzzle velocity using equation 78. The differences in the impact location can then be assessed or, alternatively, the discrete forms of the appropriate derivatives evaluated. This may be the preferred approach for practical applications due to the complicated form of the equations in the appendix. However, if the muzzle velocity is varied, there is a small effect on the muzzle retardation that should be considered because the drag coefficient varies with Mach number. Equation 101 shows the appropriate value of the retardation if the muzzle velocity is varied when performing these computations.

$$\left(\frac{dV}{ds}\right)_{V_{new}} = \left(\frac{dV}{ds}\right)_0 \left(\frac{V_0}{V_{new}}\right)^{n-1} \quad . \tag{101}$$

Note that for n = 1, the muzzle retardation does not change with muzzle velocity. This is consistent with the results presented previously in equation 35.

The variability of the impact location with muzzle velocity or muzzle retardation as a function of range can also be assessed using the series expansion in equation 93 and are shown in equations 102 and 103.

$$\frac{ds_{g-drop}}{d\left(\frac{dV}{ds}\right)_0} \cong -\frac{g}{\left(\frac{dV}{ds}\right)_0^2}\left\{-\frac{1}{3}\left[\left(\frac{dV}{ds}\right)_0 \frac{(s_x - s_{x0})}{V_0}\right]^3 + \frac{2(n+2)}{12}\left[\left(\frac{dV}{ds}\right)_0 \frac{(s_x - s_{x0})}{V_0}\right]^4 + \frac{-3(n+1)(n+2)}{30}\left[\left(\frac{dV}{ds}\right)_0 \frac{(s_x - s_{x0})}{V_0}\right]^5 + \ldots\right\} . \quad (102)$$

$$\frac{ds_{g-drop}}{dV_0} \cong -\frac{g}{V_0\left(\frac{dV}{ds}\right)_0^2}\left\{-\left[\left(\frac{dV}{ds}\right)_0 \frac{(s_x - s_{x0})}{V_0}\right]^2 + \frac{(n+2)}{3}\left[\left(\frac{dV}{ds}\right)_0 \frac{(s_x - s_{x0})}{V_0}\right]^3 - \frac{(n+2)(n+1)}{6}\left[\left(\frac{dV}{ds}\right)_0 \frac{(s_x - s_{x0})}{V_0}\right]^4 + \frac{(n+1)(n+2)(8-3n)}{30}\left[\left(\frac{dV}{ds}\right)_0 \frac{(s_x - s_{x0})}{V_0}\right]^5 + \ldots\right\} . \quad (103)$$

The results in equation 103 include the variation in the muzzle retardation due to change in muzzle velocity.

Figures 18 and 19 show the variation in impact location with changes in muzzle retardation, while figures 20 and 21 show the variation in impact location with changes in muzzle velocity. The variation in the impact location with muzzle velocity or muzzle retardation increases with increasing range. For shorter ranges, the results are relatively independent of the drag coefficient exponent and the first term of the expansions in equations 102 and 103 can be used to estimate the variability in impact location with muzzle velocity and muzzle retardation. For increased accuracy, additional terms in the series may be required. Alternatively, the analytical expressions in the appendix can be evaluated or equations 79–82 can be applied to determine the variability in impact location for different discrete values of the muzzle retardation or muzzle velocity.

## 5. Crosswind Deflection

The 2-DOF equations allow the two-dimensional trajectory of a projectile to be characterized. There are also additional physical effects that cause the projectile's trajectory to deviate from a

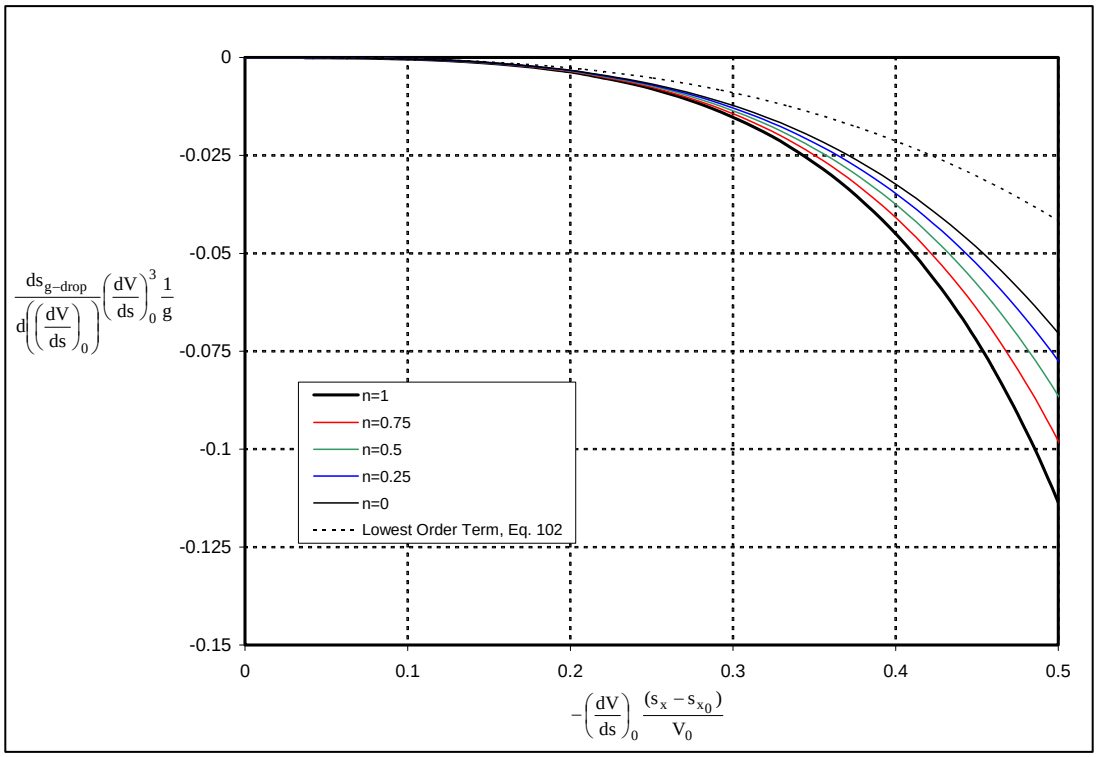


Figure 18. Scaled rate of change of vertical impact location with change in muzzle retardation as a function of scaled range.

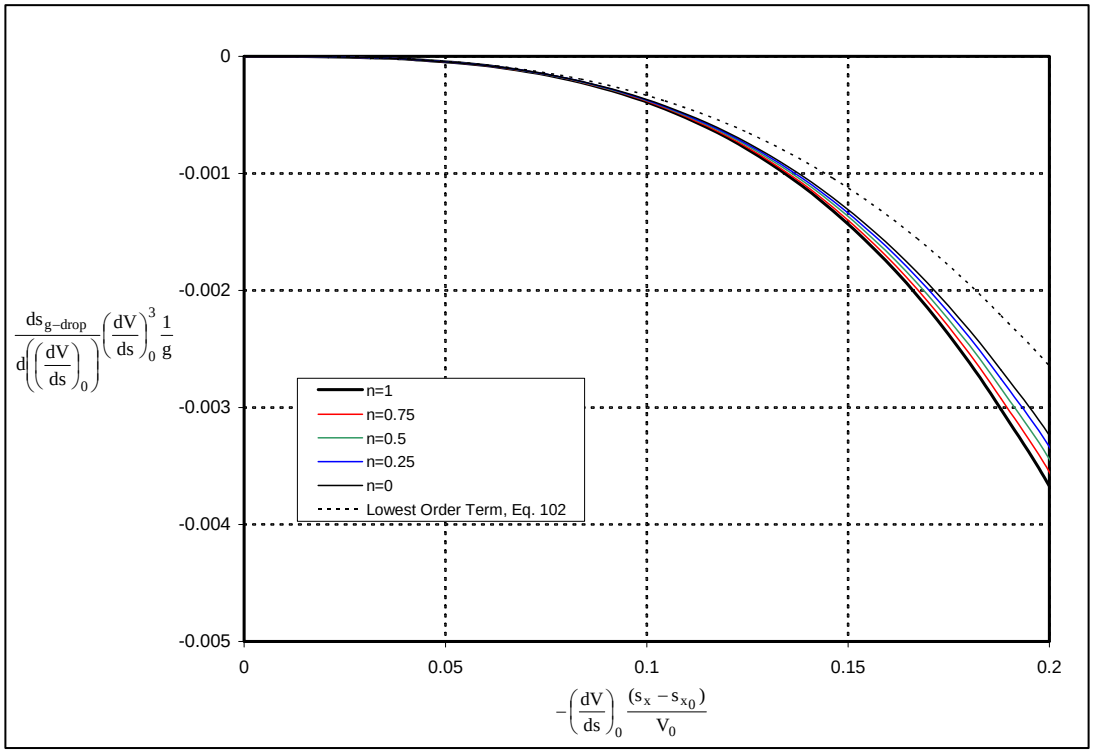


Figure 19. Scaled rate of change of vertical impact location with change in muzzle retardation as a function of scaled range (close-up).

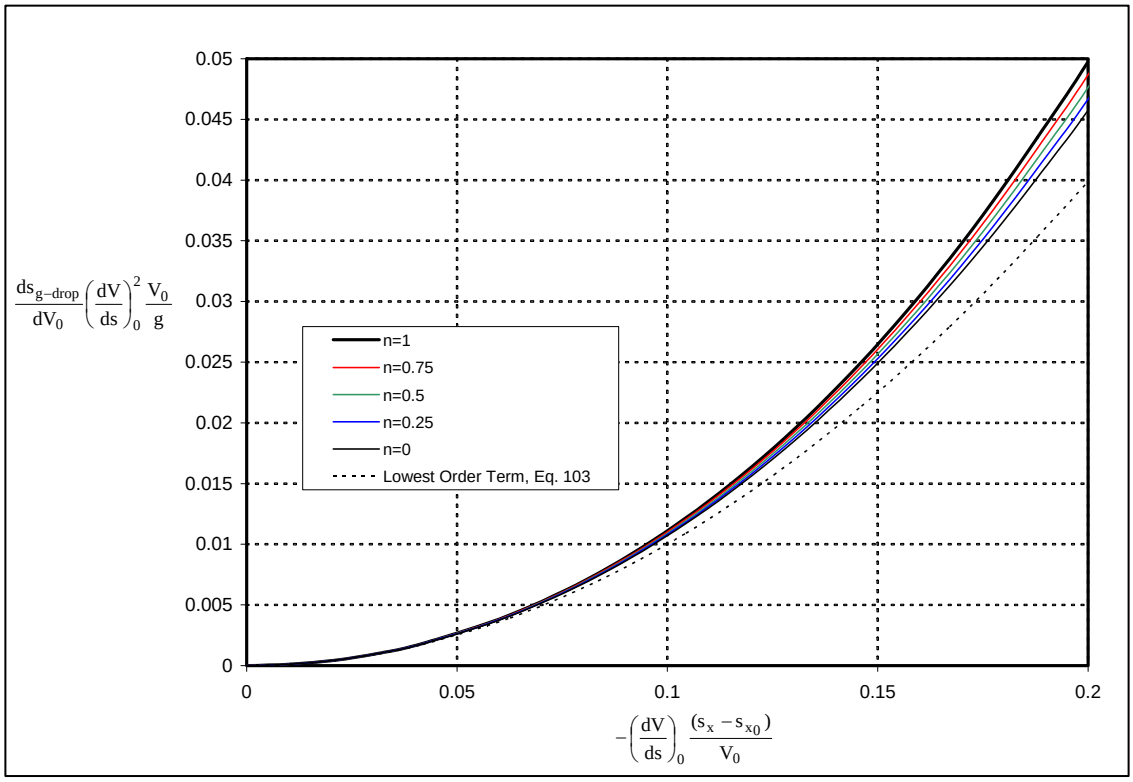


Figure 20. Scaled rate of change of vertical impact location with change in muzzle velocity as a function of scaled range.

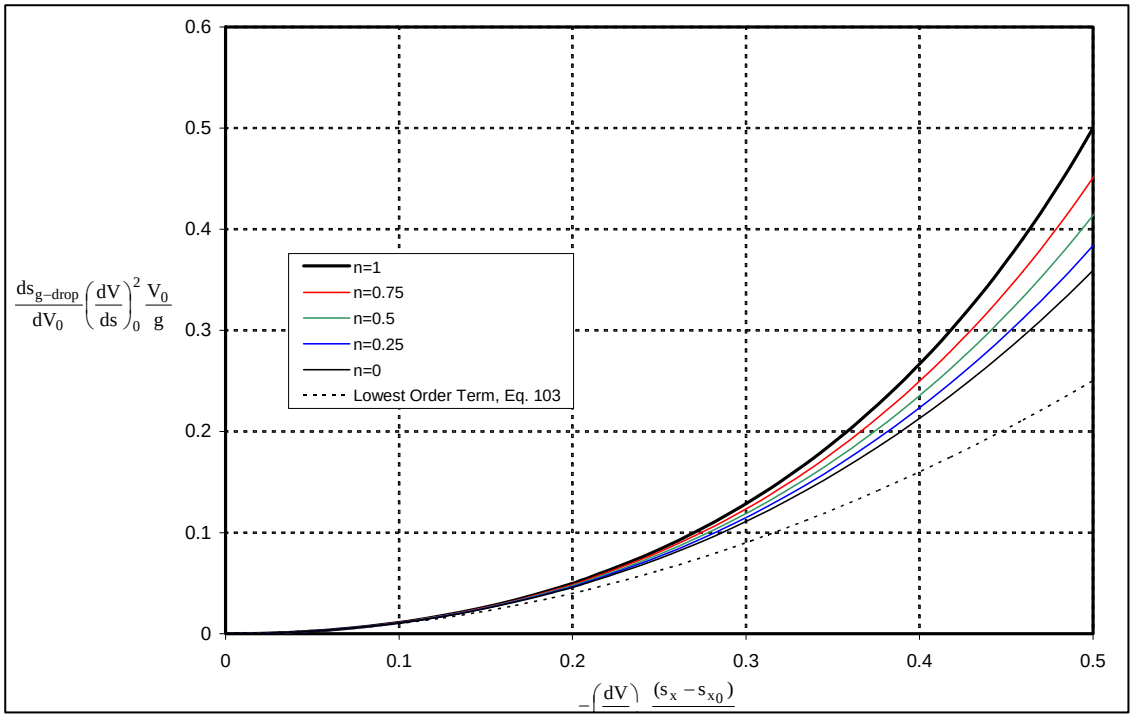


Figure 21. Scaled rate of change of vertical impact location with change in muzzle velocity as a function of scaled range (close-up).

purely two-dimensional motion. These include the crosswind drift and the drift produced by the yaw of repose that results from the interaction of the projectile's spin and the curvature of the trajectory. The drift produced by the yaw of repose is relatively small for most direct-fire munitions and, although there are aspects of the current analysis that are useful for estimating the drift, the magnitude of the drift requires additional detailed information about the aerodynamics of the munition that are beyond the scope of the current analysis.

The crosswind drift is, however, much more important for direct-fire munitions and produces a deflection horizontally away from the desired impact location in the direction of the crosswind for unboosted munitions whose velocity decreases throughout flight. The crosswind drift is also relatively easily predicted using the results presented here. The analysis requires the 3-DOF equations to be considered. However, this analysis has already been performed (*14*) and a relatively simple and very accurate expression for the crosswind drift is available and is shown in equation 104.

$$s_z - s_{z_0} = w_z \left[ (t - t_0) - \frac{(s_x - s_{x0})}{V_0} \right] . \tag{104}$$

Essentially, the crosswind deflection is proportional to the difference in actual time-of-flight and the hypothetical time-of-flight in a vacuum. Using the current analysis, the time-of-flight for direct-fire munitions can be easily determined using equations 25–27. Combining equation 104 and equations 25–27 yields an important result because it shows, for a constant crosswind, the crosswind deflection is a function of the muzzle velocity, muzzle retardation, and, to a much lesser extent, the exponent determining the shape of the drag curve. This has important implications for projectile design because the crosswind sensitivity of a munition can only be significantly effected through two design variables: muzzle velocity and muzzle retardation.

Using the expansion for time-of-flight presented in equation 39, the expansion for the crosswind deflection is easily obtained.

$$\begin{aligned} s_z - s_{z_0} = \frac{w_z}{\left(\frac{dV}{ds}\right)_0} \Bigg\{ & -\frac{1}{2}\left[\left(\frac{dV}{ds}\right)_0 \frac{(s_x - s_{x0})}{V_0}\right]^2 + \frac{1}{6}(1+n)\left[\left(\frac{dV}{ds}\right)_0 \frac{(s_x - s_{x0})}{V_0}\right]^3 + \\ & -\frac{1}{24}(1+n)(1+2n)\left[\left(\frac{dV}{ds}\right)_0 \frac{(s_x - s_{x0})}{V_0}\right]^4 + \ldots \\ & +\frac{(-1)^{j+1}}{j!}(1+n)(1+2n)\ldots(1+(j-2)n)\left[\left(\frac{dV}{ds}\right)_0 \frac{(s_x - s_{x0})}{V_0}\right]^j + \ldots \Bigg\} . \end{aligned} \tag{105}$$

The lowest-order approximation to the wind sensitivity is easily obtained from equation 105 as shown in equation 106. To lowest order, the wind sensitivity is independent of the drag coefficient exponent.

$$s_z - s_{z_0} = -\frac{w_z}{2}\left(\frac{dV}{ds}\right)_0 \frac{(s_x - s_{x0})^2}{V_0^2} \quad . \tag{106}$$

The crosswind deflection vs. scaled range is shown in figure 22. The crosswind deflection increases with increasing range. There is a relatively minor dependence on the shape of the drag curve with crosswind deflection increasing slightly with increase values of the drag coefficient exponent.

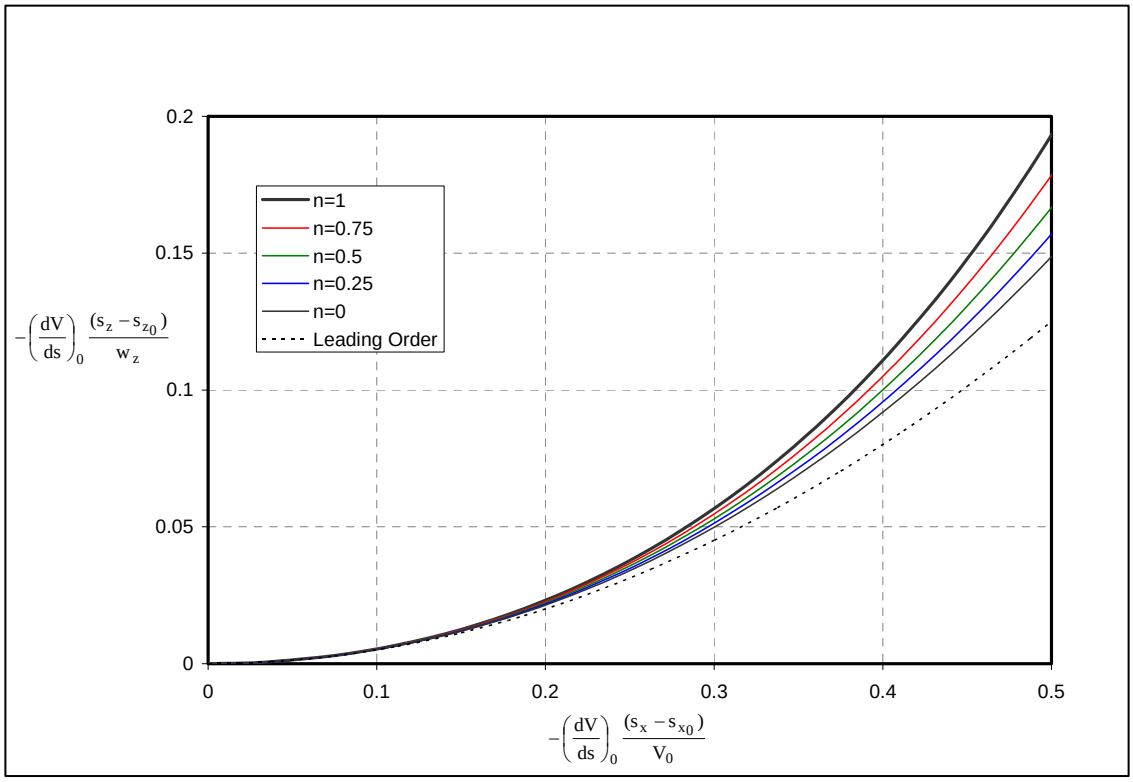


Figure 22. Crosswind deflection as a function of scaled range.

Similar simple expressions for predicting the vertical deflection due to range wind (tail or head wind) can also be found (*14*), and the range wind deflection can be related to the muzzle velocity, muzzle retardation, and exponent defining the shape of the drag curve using the results presented in the current report. However, it is also recognized that the range wind deflection is also much smaller than the crosswind deflection (*14*) and is generally ignored. For this reason, these equations are not presented here, although their development is rather straight-forward using the current analysis.

# 6. Validation

Validation of the analytical results previously presented has been performed by comparisons with numerical trajectory predictions for actual direct-fire munitions. For the current study, the 6-DOF trajectory option within the commercially-available aerodynamic analysis package Prodas was utilized.

Four projectiles were selected to perform the validation study. These include the 120-mm M829A1 KE projectile, the 120-mm M865 training round for KE projectile, and the 120-mm M830 and M830A1 HEAT munitions. The M829 presents a typical modern high mass, low drag KE projectile. The M865 and M830 are physically very different projectiles, with dissimilar muzzle velocities and retardation. However, the retardation divided by the muzzle velocity is similar. Thus, both rounds have a similar nondimensional range parameter for a given dimensional range. The M865 has a cone-cylinder fore body with a flared after body stabilizer. The M830 has a nearly full bore cylindrical mid-section with a spiked nose and a finned tail boom. Also included is the M830A1 HEAT munition. This round has a higher muzzle velocity than the M830 and lower retardation. The M830A1 has a subcaliber cylindrical mid-section with a conical nose and a finned tail boom. The muzzle velocity, muzzle retardation, and range scaling parameter for each of the projectiles is shown in table 4. The wide differences in muzzle velocity and muzzle retardation allow the effect of both of these parameters to be clearly illustrated in the following results. The exponents defining the shape of the drag curve used in the validation study for the M829A1, M865PIP, and M830A1 are listed in table 1. A drag coefficient exponent of 0.65 was used for the M830 munition to represent the shape of the drag curve over a range of Mach numbers between Mach 1.1 and 3.3.

Table 4. Projectile characteristics for validation study.

| **Projectile Type** | **Muzzle Velocity, $V_0$ (m/s)** | **Muzzle Retardation ([m/s]/km)** | $\left(\frac{dV}{ds}\right)_0 \frac{1}{V_0}$ **(1/km)** |
|---|---|---|---|
| M829A1 | 1580 | 68 | 0.043 |
| M865PIP | 1700 | 343 | 0.202 |
| M830 | 1140 | 273 | 0.239 |
| M830A1 | 1410 | 209 | 0.148 |

Most of the previous analyses examining the power-law drag formulations (*3*, *7*, and *11*) have focused on axisymmetric projectiles. The projectile geometries selected here are very diverse and show the potential of the method for addressing a wide range of projectile configurations.

Results for all four projectiles were obtained using existing inventoried Prodas models. For consistency, the drag variation with Mach number obtained from the U.S. Army Firing Tables

Branch “aeropack” data was substituted for the existing drag model within the inventoried models. The difference in the drag between the two sets of models was less than 4% over the expected Mach number regime for a 3-km flight, except for the M830 which showed differences of up to 8% near the end of the trajectory. Some additional results were obtained using the unmodified inventoried models. These additional results are discussed at the end of the validation results section.

Trajectory predictions were obtained for the baseline flight conditions for a 3-km flat-fire flight for each of the four munitions. Figure 23 show the fractional remaining velocity as a function of range. The degree of velocity loss among the four munitions increases as the ratio of retardation to velocity increases. The M865 and M830 have relatively similar performance because this ratio is similar for both rounds.

Figure 24 shows the time-of-flight as a function of range. For short ranges, the time-of-flight is dominated by the muzzle velocity and the shortest times-of-flight are produced by the highest muzzle velocities. However, as the range increases, the retardation has a more important role. For example, the M865, which has the highest muzzle velocity, has the lowest time of flight at short range, but has a time of flight similar to the M830A1 at 3 km.

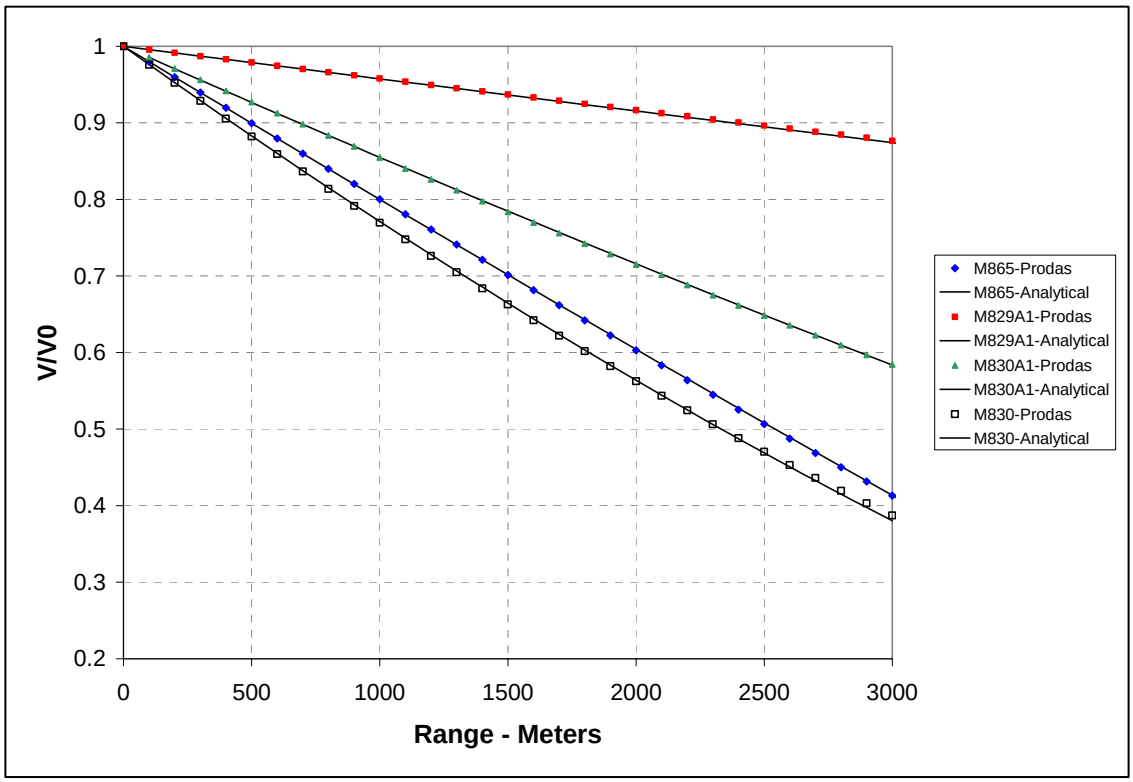


Figure 23. Fractional remaining velocity vs. range, M865PIP, M829A1, M830A1, and M830.

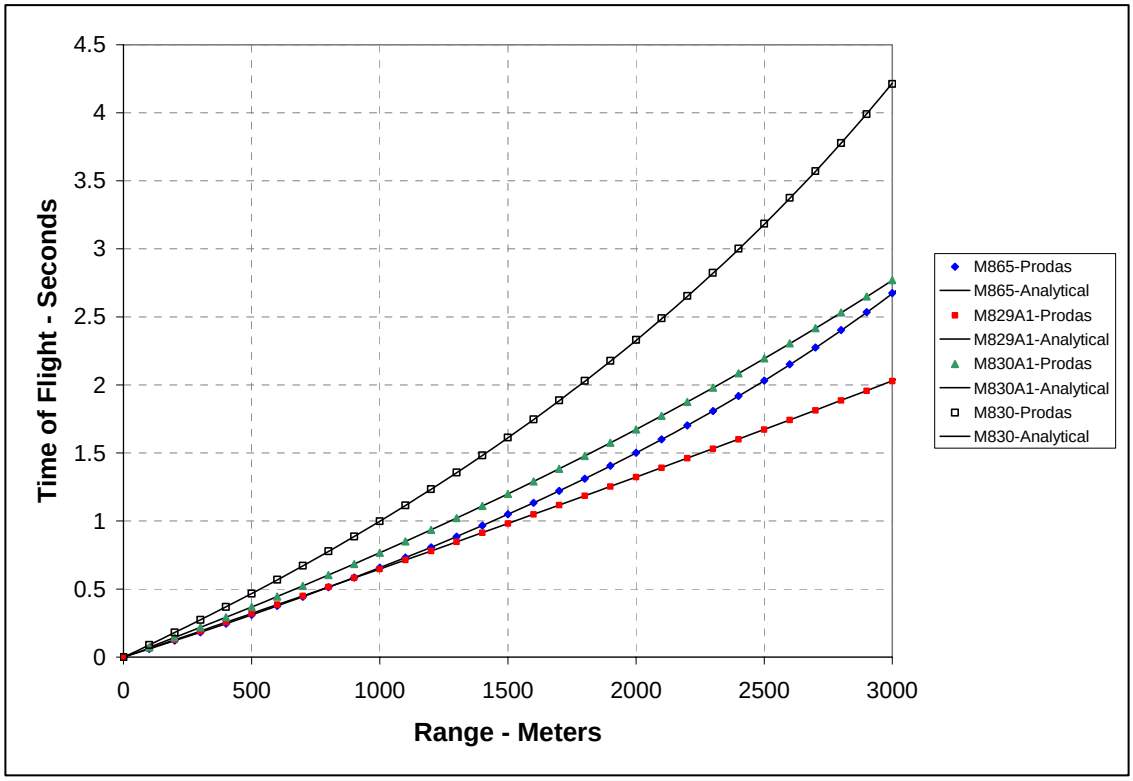


Figure 24. Time-of-flight vs. range, M865PIP, M829A1, M830A1, and M830.

The dominant effect of muzzle velocity and retardation relative to the exponent defining the shape of the drag curve is clearly illustrated in both figures 23 and 24. The effect of the exponent defining the shape of the drag curve would produce only minor deviations about each of these curves. The largest differences between the curves is produced by the values of muzzle velocity and retardation.

Figures 25 and 26 show the gravity drop and vertical displacement along the trajectory. The M829A1 has the lowest gravity drop and flattest trajectory due to its high muzzle velocity and low retardation. At ranges less than 1000 m, the gravity drop for the M829A1 and M865 are very similar because their muzzle velocities are similar. However, the curves diverge at longer ranges due to the higher retardation of the M865.

Figures 27 and 28 show the required gun elevation angle and impact angle as function of range for flat-fire trajectories. Unlike the results presented in figures 23–25, which are essentially independent of gun elevation angle, individual trajectories had to be generated using Prodas for each range location shown in figures 27 and 28. As shown in equation 95, the gun elevation angle is determined from the gravity drop. Thus, the ordering of the gun elevation angle and gravity drop results for each of the respective projectiles is very similar. For short ranges, both the gravity drop and gun elevation angle are functions primarily of the muzzle velocity. As the range increases, the role of the muzzle retardation increases. The impact angle shows similar trends to the launch angle. At short ranges, the magnitude of the impact angle is relatively close

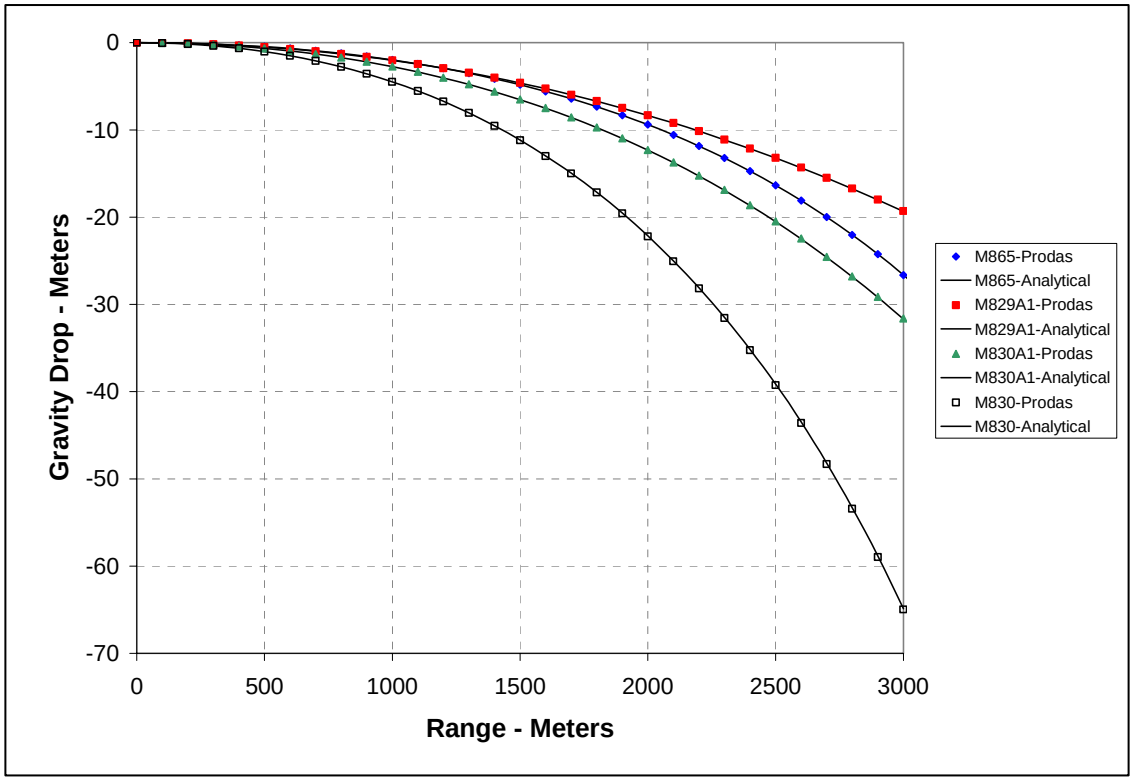


Figure 25. Gravity drop vs. range, M865PIP, M829A1, M830A1, and M830.

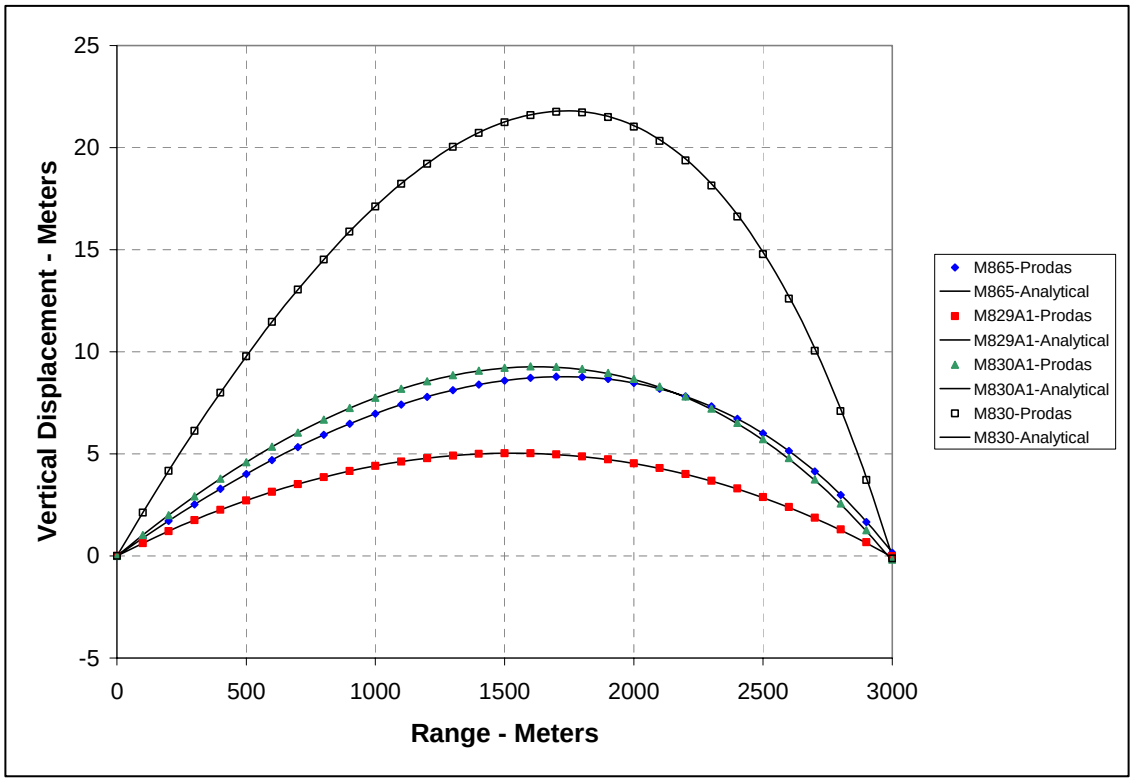


Figure 26. Trajectory to 3 km, M865PIP, M829A1, M830A1, and M830.

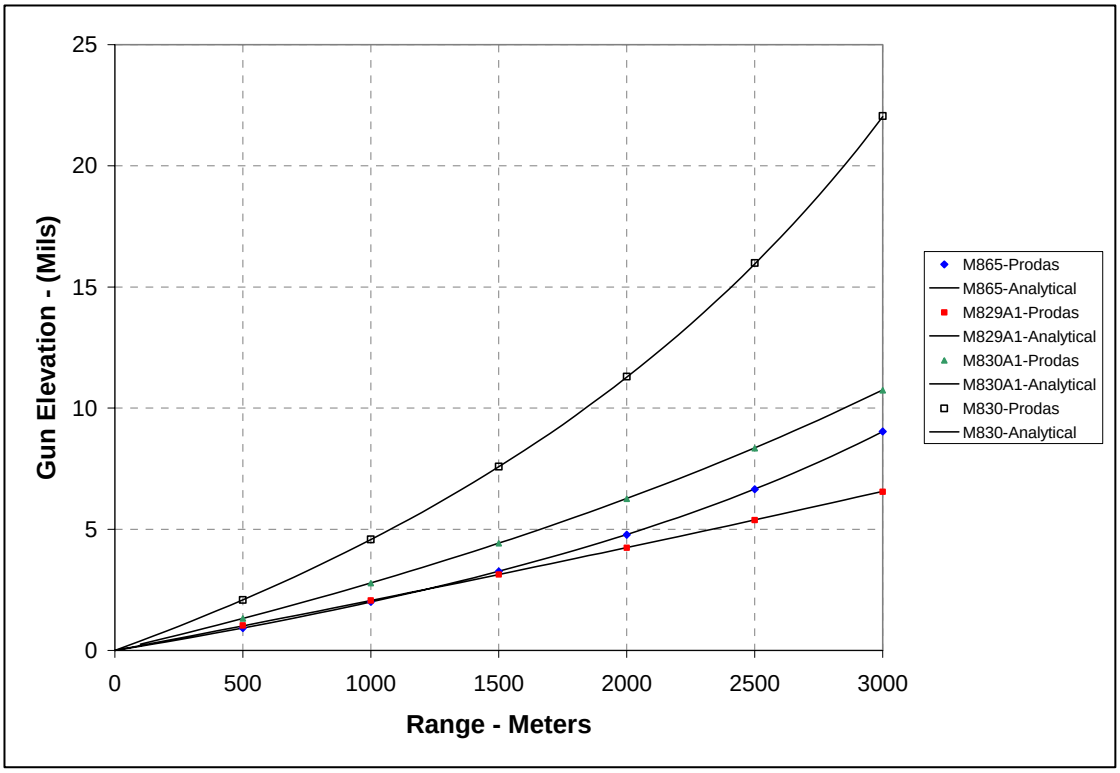


Figure 27. Gun elevation angle vs. range, M865PIP, M829A1, M830A1, and M830.

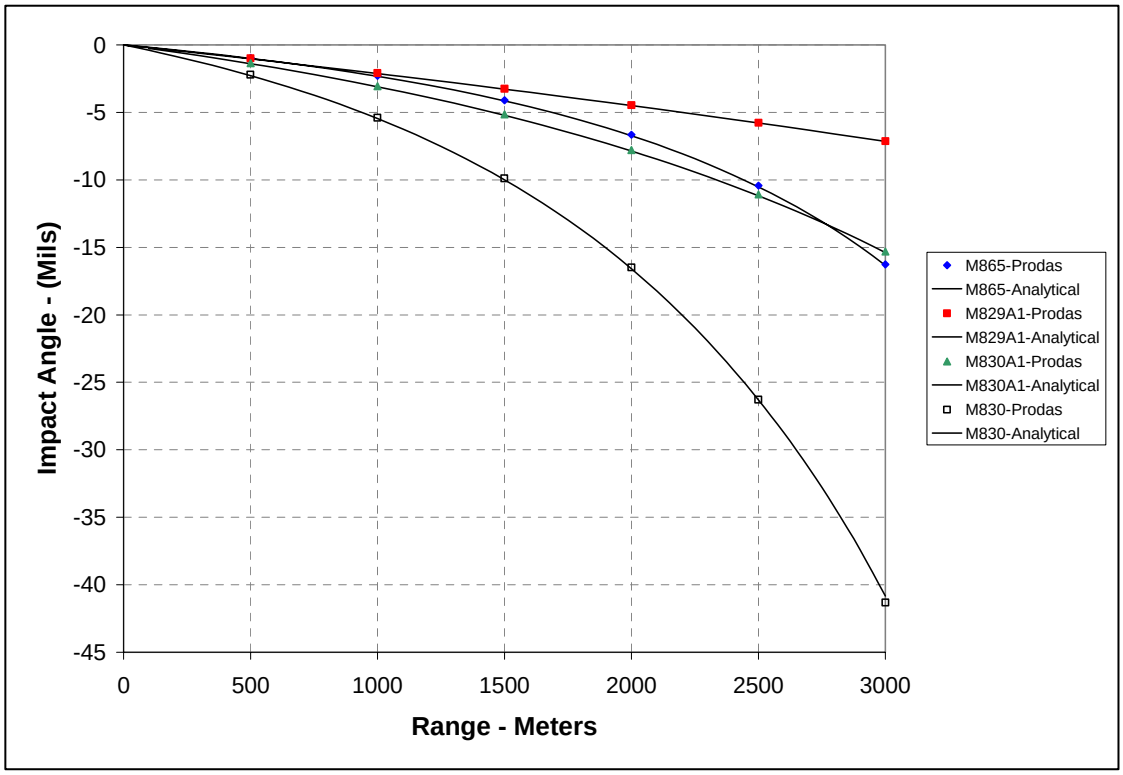


Figure 28. Impact angle vs. range, M865PIP, M829A1, M830A1, and M830.

to the gun elevation angle, but opposite in sign, as predicted from the vacuum trajectory result. As the range increases, the magnitude of the impact angle increases relative to the launch angle as a result of the increased role of the retardation in reducing the forward velocity of the projectile. Impact angle is directly related to the sensitivity of the projectile's vertical impact location to uncertainty of range-to-target estimates (also known as ranging error). The results show that the M829A1 is much less sensitive to the range estimates than the M830. The results show that a 50-m error in range estimate for the M830 results in a 2-m vertical offset in target impact location at 3000-m range.

Figure 29 shows the wind drift as a function of range for 10-m/s crosswind. While this is a relatively large crosswind velocity, the results scale linearly with wind velocity as shown in equation 104. The drift of the M829A1 is relatively small compared with the other rounds as a result of its high velocity and low retardation. Despite its higher muzzle velocity, the M865 has greater wind sensitivity than the M830A1 due to its increased retardation. Although the M830 has lower retardation than the M865, it has a larger wind sensitivity due to its lower velocity.

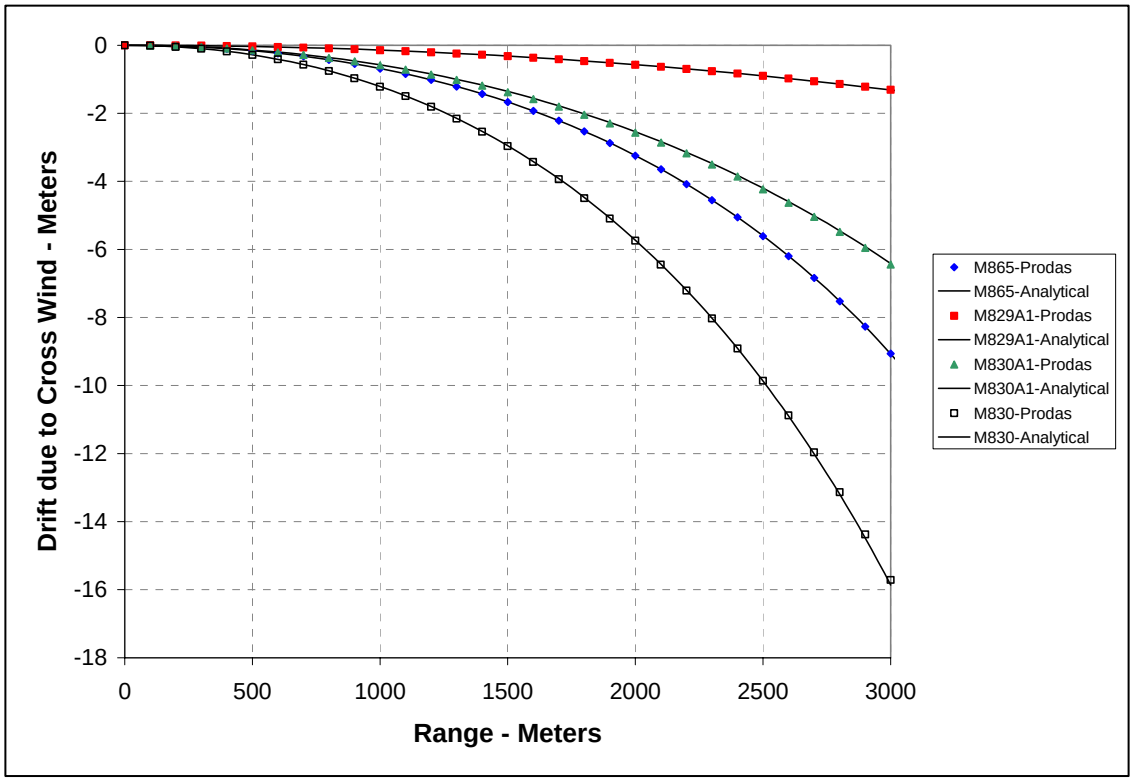


Figure 29. Wind drift vs. range for 10 m/s crosswind, M865PIP, M829A1, M830A1, and M830.

Additional results were obtained to examine the variability of the impact location to variations in muzzle velocity or muzzle retardation. For the respective sensitivity studies, the muzzle velocity was increased by 20-m/s and the retardation was increased by 5%. Although variations this large are not common for these munitions, large values were required to obtain sufficient significant digits from the Prodas output to properly determine the difference in impact location between the baseline trajectory and the perturbed trajectory. The variation of the impact location with variation in muzzle velocity appears to be relatively linear with respect to the incremental changes shown, so the results can be scaled to determined the relative change in impact for smaller changes in muzzle velocity or muzzle retardation.

Figures 30 and 31 show the difference in time-of-flight and difference in vertical impact location as a function of range produced by a 20-m/s difference in muzzle velocity. Increasing the muzzle velocity decreases the time-of-flight and produces upward movement of the target impact location. At ranges less than 1 km, the variability in impact location is relatively small, but increases, in some cases, significantly with range. The results show that the deviation of the impact location increases with increasing muzzle retardation and decreasing muzzle velocity.

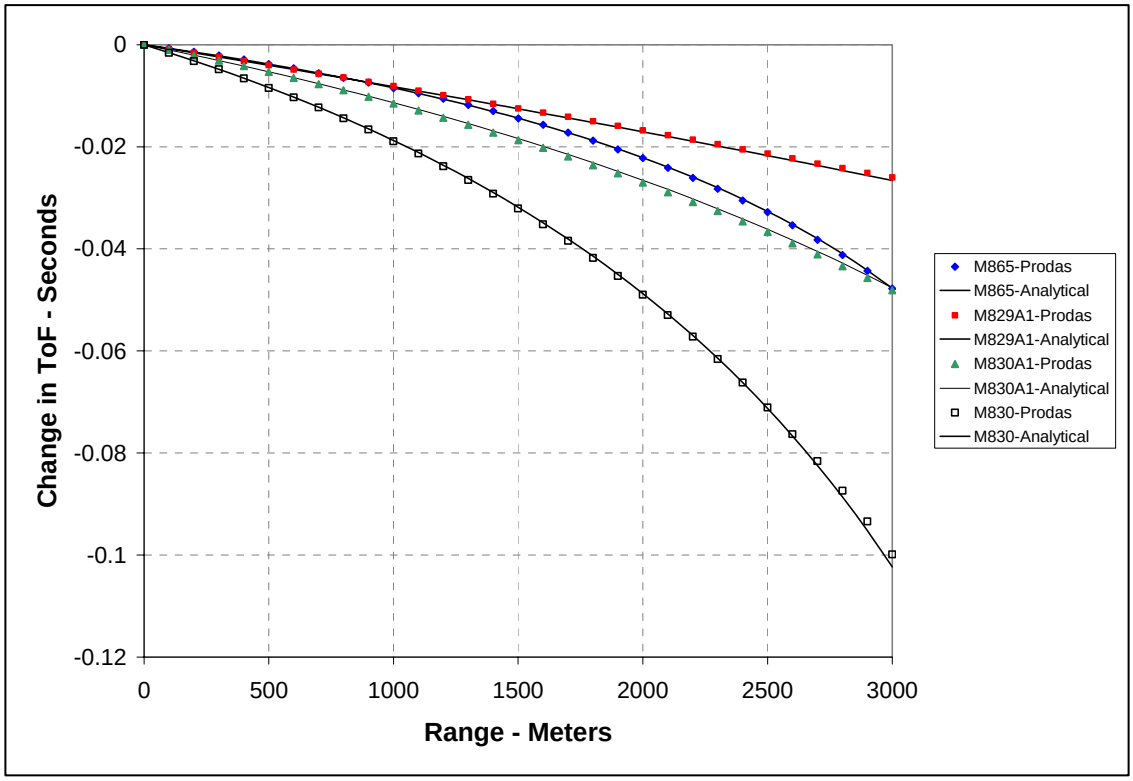


Figure 30. Change in time-of-flight vs. range for 20-m/s increase in muzzle velocity, M865PIP, M829A1, M830A1, and M830.

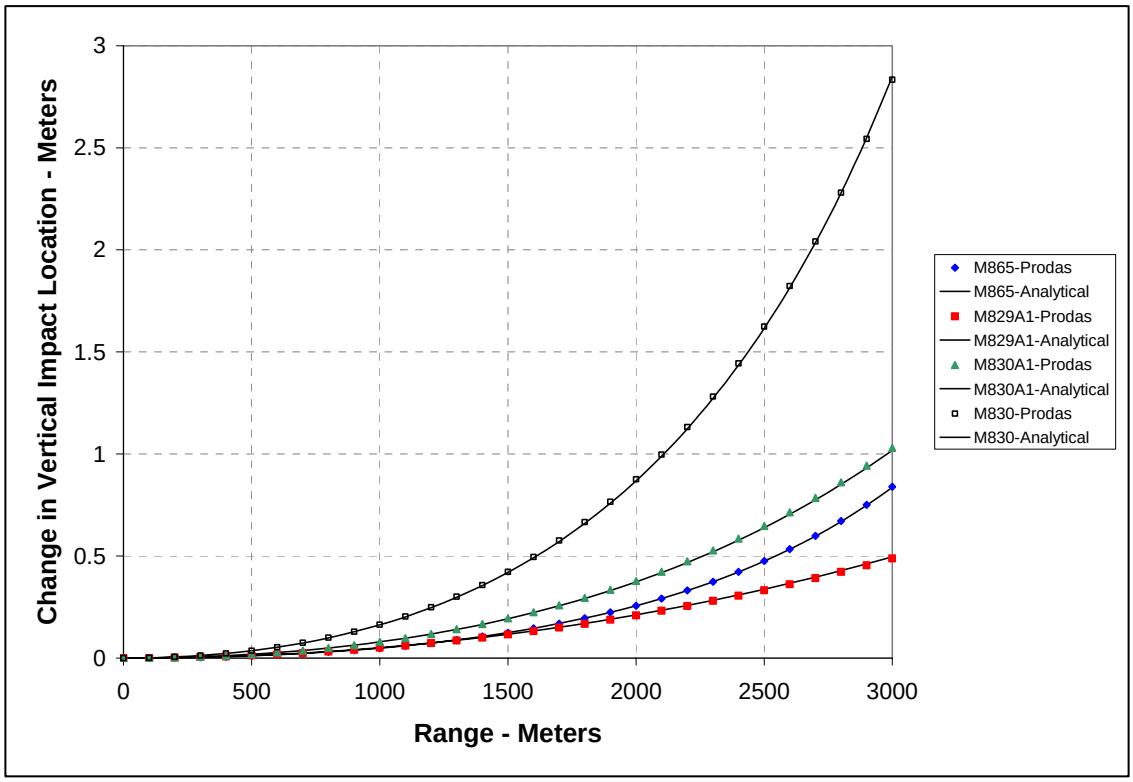


Figure 31. Change in vertical impact location vs. range for 20-m/s increase in muzzle velocity, M865PIP, M829A1, M830A1, and M830.

The results for the difference in time-of-flight and difference in vertical impact location as a function of range produced by 5% increase in muzzle retardation shown in figures 32 and 33 show a similar variation between the four projectiles. This increased drag produces lower than desired impact on the target. Changes in muzzle retardation can result from variation in the weight of the projectile, variation in drag due to geometric variations, in-bore or in-flight damage and due to variability in the atmospheric density. The current method allows each of these effects to be quantified in terms of the muzzle retardation.

It is interesting to note that although the magnitude of the change in impact location due to 20-m/s velocity increase and 5% retardation increase are similar for the M830, the same velocity increase produces more of a change in impact location for the M829A1 than the retardation increase does. This is because the gravity drop (and time-of-flight) of the M829A1 is influenced heavily by the muzzle velocity and the muzzle retardation only plays a minor role.

In general, virtually all of the results in figures 23–33 show excellent agreement between the analytical approach with a power-law drag variation and numerical prediction with the drag variation derived from experimental data. The largest differences were observed for the M830 projectile which experiences a large variation in velocity (from M = 3.3 to 1.3) across the 3-km trajectory. Although differences of about 1% between the assumed form of the drag curve and

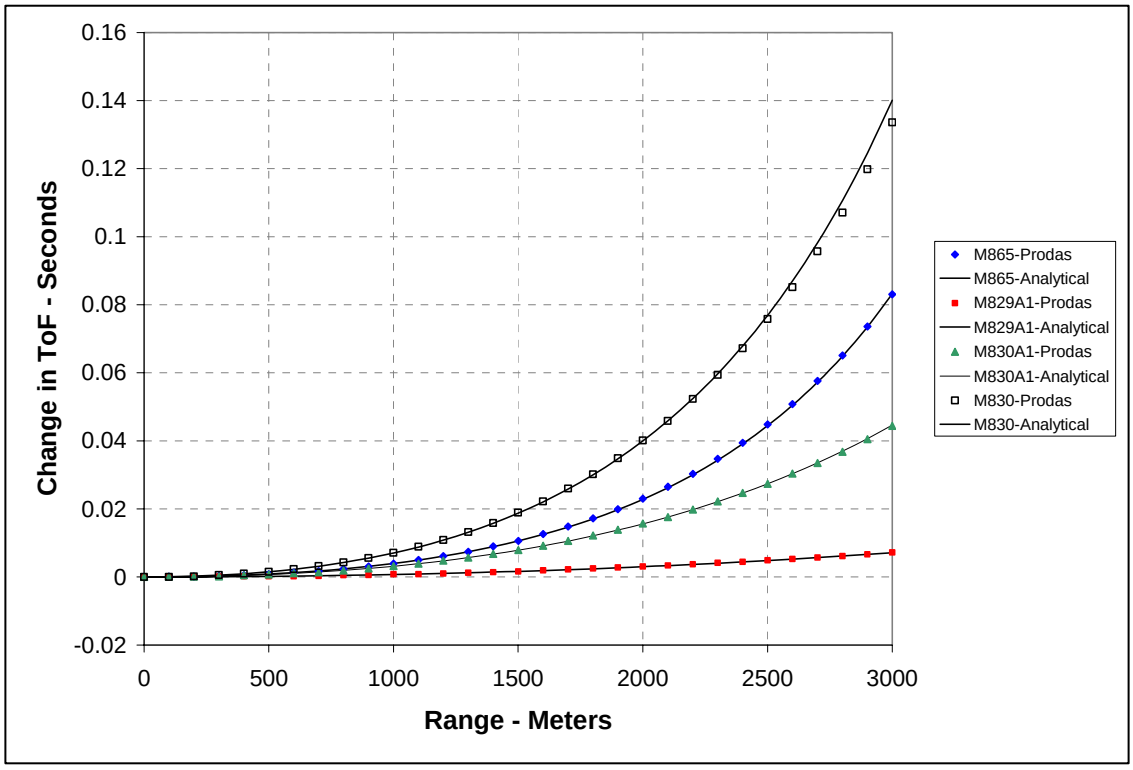


Figure 32. Change in time of flight vs. range for 5% m/s increase in muzzle retardation, M865PIP, M829A1, M830A1, and M830.

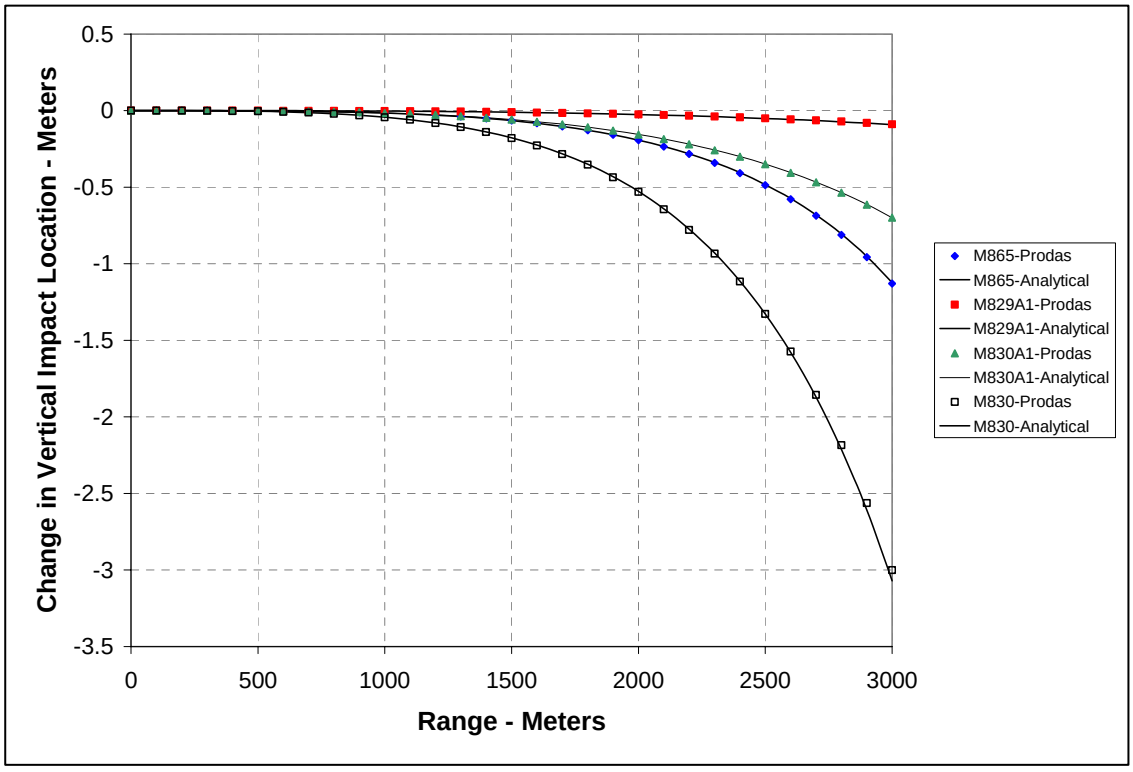


Figure 33. Change in vertical impact location vs. range for a 5% increase in muzzle retardation, M865PIP, M829A1, M830A1, and M830.

the measured drag curve were present between the launch Mach number and Mach 2, these differences increase to about 8% at the terminal Mach number. In contrast, the M865 has a similar variation in velocity on a percentage basis, but the assumed form of the drag curve agreed with the measured drag curve to within 1%. The M865 terminal Mach number was also somewhat higher, perhaps in a regime where the power-law drag variation is more applicable. The results generally validate the approach of representing the drag with a power-law approach.

Predictions were also obtained with the unmodified inventoried Prodas models for each of the four projectiles. Comparisons were made with the analytical results obtained previously. Although the results were generally in excellent agreement with the analytical model, some small differences in the results were noted. Figure 34 shows the velocity history as a function of range for each of the four projectiles and presents comparisons of the previous analytical results with the numerical results obtained using the unmodified inventoried Prodas files. Comparisons between figures 23 and 34 show that the numerical results for the M865 in figure 34 exhibit slightly less velocity fall-off relative to the analytical results than the results shown in figure 23. The opposite trend is observed for the M830A1. The differences between numerical results in figures 23 and 34 are purely due to the slight differences in the drag curves used in the numerical predictions. It is clear that uncertainty in the projectile drag effects trajectory predictions of both the analytical and numerical methods. For the numerical method, uncertainty is contained in the drag curve itself. For the analytical method, the same uncertainty exists within the muzzle retardation and exponent defining the same of the drag curve. (A similar argument can be made if there are uncertainties associated with the muzzle velocity.) The important point here is that although the power-law drag variation represents an approximation of a more general drag curve, any resulting error from this approximation in the trajectory prediction will only be meaningful if the drag curve itself is well determined. The results presented here indicate that for these projectiles, the errors from assumptions made for the analytical method are less than the errors associated with the uncertainty in the drag curve.

The results of this section provide validation of the accuracy of the method. However, it should be again emphasized that the significant value of the method is its simplicity. The results presented here were obtained using only three parameters to describe the projectile: the muzzle velocity, the muzzle retardation, and the exponent defining the shape of the drag curve. Using these parameters, a significant range of performance metrics were accurately determined. The relative effect of these parameters is clearly and easily extracted from the analysis.

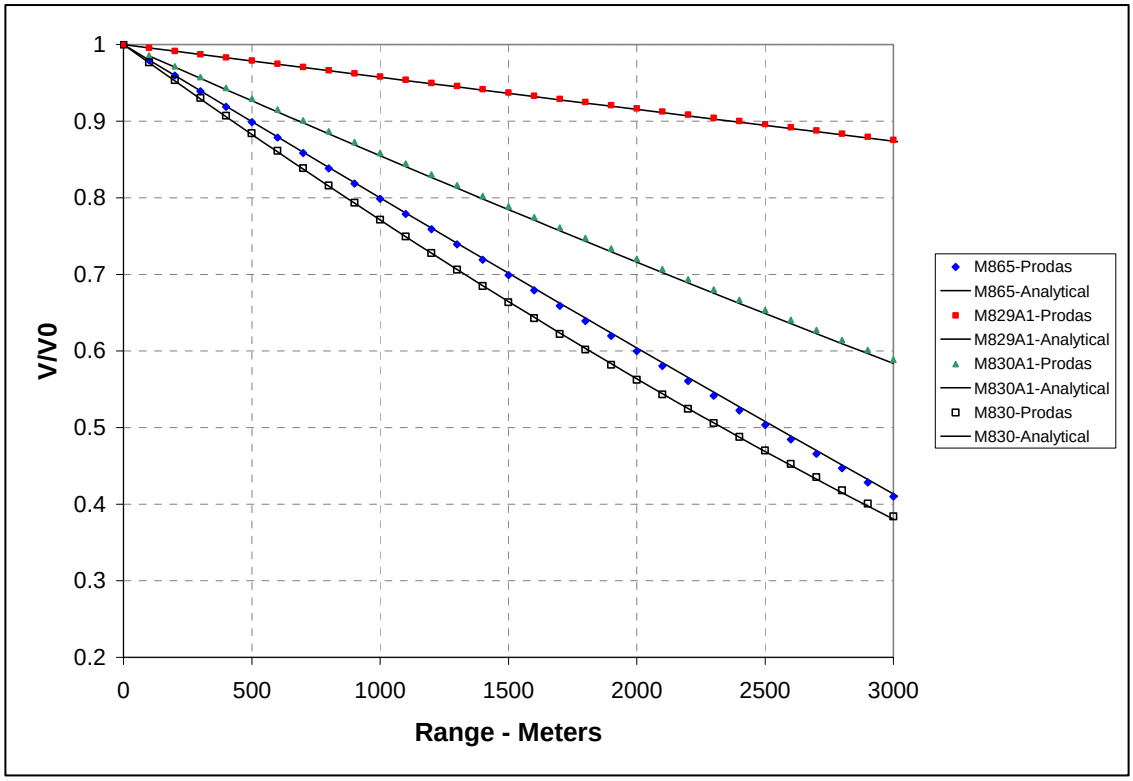


Figure 34. Fractional remaining velocity vs. range, M865PIP, M829A1, M830A1, and M830 obtained with original Prodas inventoried models.

## 7. Conclusion

An analytical approach has been developed for predicting the trajectories of high-velocity direct-fire munitions. The method is based on the flat-fire point-mass equations of motion with a specific functional form for the variation of the drag coefficient with Mach number. Using this approach, analytical solutions of the equations of motion have been obtained and the displacement and velocity along the trajectory has been determined. The analysis demonstrates that the munition can be characterized in terms of three parameters; the muzzle velocity, the muzzle retardation, and a single parameter defining the shape of the drag curve. Drag data for modern high-velocity direct-fire munitions has been analyzed and the expected range of the parameter defining the shape of the drag curve has been determined. The analysis of the predicted trajectories shows that the muzzle velocity and the muzzle retardation are the dominant variables and the parameter defining the shape of the drag curve is a higher-order term which, in some cases, can be ignored.

The method has been validated with numerical trajectory predictions for four modern direct-fire munitions. Excellent agreement is found between the two methods. The errors associated with the approximations required to obtain analytical solutions are relatively small, particularly when

one considers the uncertainty (or naturally occurring variability) associated with the drag coefficient (or even muzzle velocity) for a given munition.

There are numerous applications for the method. The simplicity and accuracy of the method make it appropriate for use in preliminary design studies where the prediction of munition performance may be desired but where details of the design have not been completely defined. The method also has important implications for munition accuracy testing and analysis. The method provides a formal framework for constructing error budgets, and determining variance components and their associated scale factors. The method also allows for improved analysis of target impact data from jump tests by allowing improved corrections due to gravity drop and variability due muzzle velocity and retardation. The technique may also be useful for direct-fire smart munition guidance, navigation, and control (GN&C) applications where speed and simplicity of the GN&C algorithm may reduce the demands on the onboard electronic package. Some of these applications are currently being exploited.

## 8. References


1. Mayevski, N. V. *Traité de balistique extérieure*; Gauthier-Villars: Paris, 1872.
2. Hayes, T. J. *Elements of Ordnance*; John Wiley & Sons, Inc.: New York, NY, 1938.
3. McCoy, R. L. *Modern Exterior Ballistics*, Schiffer Military History: Atglen, PA, 1999.
4. Arrow Tech Associates. *Prodas Users Manual*; Arrow Tech Associates: Burlington, VT, 2002.
5. Moore, F. G.; Hymer, T. C. *The 2002 Version of the Aeroprediction Code: Part I – Summary of New Theoretical Methodology*; NSWCDD/TR-01/108; Naval Surface Warfare Center: Dahlgren, VA, March 2002.
6. McShane, E. J.; Kelley, J. L.; Reno, F. V. *Exterior Ballistics*; The University of Denver Press: Denver, CO, 1953.
7. Pejsa, A. J. *Modern Practical Ballistics*; 2nd Ed.; Kenwood Publishing: Minneapolis, MN, 1991.
8. Tschappat, W. H. *Text-Book of Ordnance and Gunnery*; John Wiley & Sons, Inc.: New York, NY, 1917.
9. Bliss, G. A. *Mathematics for Exterior Ballistics*; John Wiley & Sons, Inc.: New York, NY, 1944.
10. Anonymous. *Handbook on Weaponry*; 2nd English Ed.; Rheinmetall GmbH: Düsseldorf, 1982.
11. Thomas, R. N. *Some Comments on the Form of the Drag Coefficient at Supersonic Velocity*; report no. 542; U.S. Army Ballistic Research Laboratory: Aberdeen Proving Ground, MD, April 1945.
12. Celmins, I. *Projectile Supersonic Drag Characteristics*; BRL-MR-3843; U.S. Army Ballistic Research Laboratory: Aberdeen Proving Ground, MD, July 1990.
13. Herrmann, E. E. *Exterior Ballistics 1935*; U.S. Naval Institute: Annapolis, MD, 1935.
14. McCoy, R. L. *The Effects of Wind on Flat-Fire Trajectories*; report no. 1900; U.S. Army Ballistic Research Laboratory: Aberdeen Proving Ground, MD, August 1976.

# Appendix. Variation in Impact Location With Change in Muzzle Retardation and Velocity Data

The variation of impact location for a fixed range with change in muzzle retardation or muzzle velocity can be obtained by computing the derivatives in equations 99 and 100. The results are shown in the following equations.

## A.1 Variation in Impact Location With Change in Muzzle Retardation

The following equations show the variation in impact location with change in muzzle retardation as a function of range for various values of the drag coefficient exponent.

$n \neq 0,1,2$

$$\frac{d s_y^P}{d\left(\frac{dV}{ds}\right)_0} = \frac{g}{(n-2)(n-1)\left(\frac{dV}{ds}\right)_0^3}\left[\left\{1+n\left(\frac{dV}{ds}\right)_0\frac{(s_x-s_{x0})}{V_0}\right\}^{\frac{2(n-1)}{n}} -1-2(n-1)\left(\frac{dV}{ds}\right)_0\frac{(s_x-s_{x0})}{V_0}\right] - \frac{g}{(n-2)\left(\frac{dV}{ds}\right)_0^3}\left[\left(\frac{dV}{ds}\right)_0\frac{(s_x-s_{x_0})}{V_0}\left\{1+n\left(\frac{dV}{ds}\right)_0\frac{(s_x-s_{x_0})}{V_0}\right\}^{\frac{n-2}{n}} -\left(\frac{dV}{ds}\right)_0\frac{(s_x-s_{x_0})}{V_0}\right] \quad . \tag{A-1}$$

$n = 0$

$$\frac{d s_y^P}{d\left(\frac{dV}{ds}\right)_0} = \frac{g}{2\left(\frac{dV}{ds}\right)_0^3}\left(2\left(\frac{dV}{ds}\right)_0\frac{(s_x-s_{x0})}{V_0}+\exp\left\{-2\left(\frac{dV}{ds}\right)_0\frac{(s_x-s_{x0})}{V_0}\right\}-1\right) - \frac{g}{4\left(\frac{dV}{ds}\right)_0^3}\left(2\left(\frac{dV}{ds}\right)_0\frac{(s_x-s_{x0})}{V_0}\left(1-\exp\left\{-2\left(\frac{dV}{ds}\right)_0\frac{(s_x-s_{x0})}{V_0}\right\}\right)\right) \quad . \tag{A-2}$$

n = 1

$$\frac{d s_y^P}{d\left(\frac{dV}{ds}\right)_0} = \frac{-2g}{\left(\frac{dV}{ds}\right)_0^3}\left( -\left(\frac{dV}{ds}\right)_0 \frac{(s_x - s_{x0})}{V_0} + \ln\left\{1+\left(\frac{dV}{ds}\right)_0 \frac{(s_x - s_{x0})}{V_0}\right\}\right)$$

$$+\frac{g}{\left(\frac{dV}{ds}\right)_0^3}\left[\frac{-\left(\left(\frac{dV}{ds}\right)_0 \frac{(s_x - s_{x0})}{V_0}\right)^2}{1+\left(\frac{dV}{ds}\right)_0 \frac{(s_x - s_{x0})}{V_0}}\right] \quad . \qquad \text{(A-3)}$$

n = 2

$$s_y^P = \frac{g}{2\left(\frac{dV}{ds}\right)_0^3}\left[\left(1+2\left(\frac{dV}{ds}\right)_0 \frac{(s_x - s_{x0})}{V_0}\right)\ln\left(1+2\left(\frac{dV}{ds}\right)_0 \frac{(s_x - s_{x0})}{V_0}\right)\right.$$

$$\left. -2\left(\frac{dV}{ds}\right)_0 \frac{(s_x - s_{x0})}{V_0}\right]$$

$$-\frac{g}{4\left(\frac{dV}{ds}\right)_0^3}\left[\left(2\left(\frac{dV}{ds}\right)_0 \frac{(s_x - s_{x_0})}{V_0}\right)\ln\left(1+2\left(\frac{dV}{ds}\right)_0 \frac{(s_x - s_{x_0})}{V_0}\right)\right] \quad . \qquad \text{(A-4)}$$

### A.2 Variation in Impact Location With Change in Muzzle Velocity

The following equations show the variation in impact location for a fixed range with change in muzzle retardation as a function of range for various values of the drag coefficient exponent. The variation in the muzzle retardation with change in muzzle velocity is also required and can be obtained using equation A-5.

$$\frac{d\left(\frac{dV}{ds}\right)_0}{dV_0} = (1-n)\frac{1}{V_0}\left(\frac{dV}{ds}\right)_0 \quad . \qquad \text{(A-5)}$$

$n \neq 0,1,2$

$$\frac{ds_{g-drop}}{d\left(\frac{dV}{ds}\right)_0} = \frac{ds_{g-drop}}{d\left(\frac{dV}{ds}\right)_0}\frac{d\left(\frac{dV}{ds}\right)_0}{dV_0} + \frac{g}{(n-2)\left(\frac{dV}{ds}\right)_0^2 V_0}\left[\left(\frac{dV}{ds}\right)_0 \frac{(s_x - s_{x0})}{V_0}\left\{\left(1 + n\left(\frac{dV}{ds}\right)_0 \frac{(s_x - s_{x0})}{V_0}\right)^{\frac{n-2}{n}} - 1\right\}\right] \quad \text{.(A-6)}$$

$n = 0$

$$\frac{ds_{g-drop}}{d\left(\frac{dV}{ds}\right)_0} = \frac{ds_{g-drop}}{d\left(\frac{dV}{ds}\right)_0}\frac{d\left(\frac{dV}{ds}\right)_0}{dV_0} + \frac{g}{4\left(\frac{dV}{ds}\right)_0^2 V_0}\left[2\left(\left(\frac{dV}{ds}\right)_0 \frac{(s_x - s_{x0})}{V_0}\right)\left(1 - \exp\left(-2\left(\frac{dV}{ds}\right)_0 \frac{(s_x - s_{x0})}{V_0}\right)\right)\right] . \quad \text{(A-7)}$$

$n = 1$

$$\frac{ds_{g-drop}}{d\left(\frac{dV}{ds}\right)_0} = \frac{ds_{g-drop}}{d\left(\frac{dV}{ds}\right)_0}\frac{d\left(\frac{dV}{ds}\right)_0}{dV_0} + \frac{g}{\left(\frac{dV}{ds}\right)_0^2 V_0}\left[\frac{\left(\left(\frac{dV}{ds}\right)_0 \frac{(s_x - s_{x0})}{V_0}\right)^2}{1 + \left(\frac{dV}{ds}\right)_0 \frac{(s_x - s_{x0})}{V_0}}\right] . \quad \text{(A-8)}$$

n = 2

$$\frac{ds_{g-drop}}{d\left(\frac{dV}{ds}\right)_0} = \frac{ds_{g-drop}}{d\left(\frac{dV}{ds}\right)_0}\frac{d\left(\frac{dV}{ds}\right)_0}{dV_0} + \frac{g}{2\left(\frac{dV}{ds}\right)_0^2 V_0}\left[\left(\frac{dV}{ds}\right)_0 \frac{(s_x - s_{x0})}{V_0} \ln\left(1 + 2\left(\frac{dV}{ds}\right)_0 \frac{(s_x - s_{x0})}{V_0}\right)\right] . \qquad \text{(A-9)}$$

## List of Symbols, Abbreviations, and Acronyms

| | |
|---|---|
| $C_D$ | Drag coefficient |
| $C_D\big\|_{V_0}$ | Drag coefficient evaluated at the muzzle velocity |
| D | Reference diameter |
| g | Gravitational acceleration |
| j | Order of term in Taylor's series expansion |
| m | Projectile mass |
| M | Mach number |
| n | Exponent defining shape of the drag vs. Mach number curve |
| s | Arc length along projectile trajectory |
| $\bar{s}$ | Arc length along trajectory in absence of gravity |
| $s_{g-drop}$ | Gravity drop |
| $s_x, s_y$ | Horizontal and vertical displacement along trajectory |
| $s_y^P$ | Particular solution associated with vertical displacement (or gravity drop) |
| $s_{x_0}, s_{y_0}$ | Initial horizontal and vertical displacement along trajectory |
| $s_z$ | Out-of-plane displacement along trajectory (normal to *x*-*y* plane) |
| $s_{z_0}$ | Initial out-of-plane displacement along trajectory |
| $S_{ref}$ | Reference area, $S_{ref} = \frac{\pi D^2}{4}$ |
| t | Time |
| $t_0$ | Initial time |
| V | Total velocity |
| $\bar{V}$ | Velocity along trajectory in absence of gravity |
| $V_0$ | Muzzle velocity |

$V_{new}$ Perturbed value of velocity in velocity sensitivity analysis

$V_x, V_y$ Horizontal and vertical component of velocity

$V_y^P$ Particular solution associated with vertical velocity

$\left(\frac{dV}{ds}\right)$ Instantaneous value of retardation along trajectory

$\left(\frac{dV}{ds}\right)_0$ Muzzle retardation

$w_z$ Crosswind velocity

Greek Symbols

$\theta_0$ Initial gun elevation angle

$\theta_I$ Trajectory impact angle

$\rho$ Atmospheric density

NO. OF
COPIES ORGANIZATION

1 (PDF ONLY) DEFENSE TECHNICAL INFORMATION CTR
DTIC OCA
8725 JOHN J KINGMAN RD
STE 0944
FORT BELVOIR VA 22060-6218

1 US ARMY RSRCH DEV & ENGRG CMD
SYSTEMS OF SYSTEMS INTEGRATION
AMSRD SS T
6000 6TH ST STE 100
FORT BELVOIR VA 22060-5608

1 INST FOR ADVNCD TCHNLGY
THE UNIV OF TEXAS
AT AUSTIN
3925 W BRAKER LN STE 400
AUSTIN TX 78759-5316

1 DIRECTOR
US ARMY RESEARCH LAB
IMNE ALC IMS
2800 POWDER MILL RD
ADELPHI MD 20783-1197

3 DIRECTOR
US ARMY RESEARCH LAB
AMSRD ARL CI OK TL
2800 POWDER MILL RD
ADELPHI MD 20783-1197

3 DIRECTOR
US ARMY RESEARCH LAB
AMSRD ARL CS IS T
2800 POWDER MILL RD
ADELPHI MD 20783-1197

ABERDEEN PROVING GROUND

1 DIR USARL
AMSRD ARL CI OK TP (BLDG 4600)

NO. OF COPIES ORGANIZATION

1 ARROW TECH ASSOCIATES
W HATHAWAY
1233 SHELBURNE RD D 8
SOUTH BURLINGTON VT 05403

1 OREGON STATE UNIVERSITY
DEPT OF MECH ENGRNG
M COSTELLO
CORVALLIS OR 97331

1 PRODUCT MANAGER
SML AND MED CAL AMMO
SFAE AMO MAS SMC
BLDG 354
LTC M BULTER
PICATINNY ARSENAL NJ 07806-5000

1 PROJECT MANAGER MANEUVER
AMMUNITION SYSTEMS
SFAE AMO MAS SMC
BLDG 354
R KOWALSKI
PICATINNY ARSENAL NJ 07806-5000

1 ATK
R DOHRN
MN11 LW1428
4700 NATHAN LANE N
PLYMOUTH MN 55442

1 ATK
C AAKHUS
MN11 2830 LW54
4700 NATHAN LANE N
PLYMOUTH MN 55442

1 ATK
M JANTSCHER, MN07 LW54
4700 NATHAN LANE N
PLYMOUTH MN 55442

1 ATK LAKE CITY
K ENLOW
PO BOX 1000
INDEPENDENCE MO 64051-1000

5 ATK
LAKE CITY SML CAL AMMO
LAKE CITY ARMY AMMO PLANT
D MANSFIELD
PO BOX 1000
INDEPENDENCE MO 64051-1000

NO. OF COPIES ORGANIZATION

1 ATK LAKE CITY SML CAL AMMO
MO10 003
LAKE CITY ARMY AMMO PLANT
J WESTBROOK
PO BOX 1000
INDEPENDENCE MO 64051-1000

1 ALLIANT TECHSYSTEMS INC.
MN07 LW54
D KAMDAR
4700 NATHAN LANE N
PLYMOUTH MN 55442-2512

1 ATK ORDNANCE SYSTEMS
MN07 MW44
B BECKER
4700 NATHAN LANE N
PLYMOUTH MN 55442-2512

1 US ARMY TACOM ARDEC
CCAC AMSTA AR CCL C
G FLEMING
BLDG 65N
PICATINNY ARSENAL NJ 07806-5000

1 US ARMY TACOM ARDEC
CCAC AMSTA AR CCL B
J MIDDLETON
BLDG 65N
PICATINNY ARSENAL NJ 07806-5000

1 US ARMY TACOM ARDEC
ASIC PROG INTEGRATION OFF
J RESCH
BLDG 1
PICATINNY ARSENAL NJ 07801

1 US ARMY TACOM ARDEC
M MINISI
BLDG 65
PICATINNY ARSENAL NJ 07806-5000

1 US ARMY TACOM ARDEC
S SPICKERT FULTON
BLDG 65N
PICATINNY ARSENAL NJ 07806-5000

1 US ARMY TACOM ARDEC
M NICOLICH
BLDG 65S
PICATINNY ARSENAL NJ 07806-5000

NO. OF COPIES ORGANIZATION

1 US ARMY TACOM ARDEC
AMSTA AR CCH A
S MUSALLI
BLDG 65S
PICATINNY ARSENAL NJ 07806-5000

1 US ARMY TACOM ARDEC
AMSRD AAR AEM I
R MAZESKI
BLDG 65N
PICATINNY ARSENAL NJ 07806-5000

1 US ARMY TACOM ARDEC
A FARINA
BLDG 95
PICATINNY ARSENAL NJ 07806-5000

1 US ARMY TACOM ARDEC
CCAC
AMSTA AR CCL B
D CONWAY
BLDG 65N
PICATINNY ARSENAL NJ 07806-5000

1 US ARMY TACOM ARDEC
AMSTA AR FSF T
H HUDGINS
BLDG 382
PICATINNY ARSENAL NJ 07806-5000

1 US ARMY TACOM ARDEC
CCAC AMSTA AR CCL D
F HANZL
BLDG 354
PICATINNY ARSENAL NJ 07806-5000

1 US ARMY TACOM ARDEC
P RIGGS
BLDG 65N
PICATINNY ARSENAL NJ 07806-5000

1 OPM MAS
SFAE AMO MAS MC
G DEROSA
BLDG 354
PICATINNY ARSENAL NJ 07806-5000

1 COMMANDER
US ARMY TACOM ARDEC
AMSTR AR FSF X
W TOLEDO
BLDG 95 S
PICATINNY ARSENAL NJ 07806-5000

NO. OF COPIES ORGANIZATION

1 AEROPREDICTION INC
F MOORE
9449 GROVER DRIVE SUITE 201
KING GEORGE VA 22485

1 US ARMY AMRDEC
AMSAM RD SS AT
R KRETZSCHMAR
BLDG 5400
REDSTONE ARSENAL AL 35898-5000

ABERDEEN PROVING GROUND

2 COMMANDER
US ARMY ARDEC
FIRING TABLES AND
BALLISTICS DIV
AMSRD AAR AEF T
B TILGHMAN
2201 ABERDEEN BLVD
APG MD 21005-5001

1 COMMANDER
US ARMY ARDEC
FIRING TABLES AND
BALLISTICS DIV
AMSRD AAR AEF T
F MIRABELLE
2201 ABERDEEN BLVD
APG MD 21005-5001

29 DIR USARL
AMSRD ARL WM B
T KOGLER
AMSRD ARL WM BA
D LYON
AMSRD ARL WM BC
M BUNDY
G COOPER (3 CPS)
J DESPIRITO
J GARNER
B GUIDOS
K HEAVEY
J NEWILL (3 CPS)
P PLOSTINS
J SAHU
S SILTON
D WEBB
P WEINACHT (3 CPS)

NO. OF
COPIES ORGANIZATION

AMSRD ARL WM BD
B FORCH
P CONROY
A ZIELINSKI
AMSRD ARL WM BF
S WILKERSON
R PEARSON
W OBERLE
AMSRD ARL WM TA
M BURKINS
AMSRD ARL WM TC
B PETERSON
L MAGNESS